

Deconfined pseudocriticality in a model spin-1 quantum antiferromagnet

Vikas Vijigiri,¹ Sumiran Pujari,^{1,*} and Nisheeta Desai²

¹*Department of Physics, Indian Institute of Technology Bombay, Powai, Mumbai, MH 400076, India*

²*Department of Theoretical Physics, Tata Institute of Fundamental Research, Colaba, Mumbai, MH 400005, India*

Berry phase interference arguments that underlie the theory of deconfined quantum criticality (DQC) for $S = 1/2$ antiferromagnets have also been invoked to allow for continuous transitions in $S = 1$ magnets including a Néel to (columnar) valence bond solid (cVBS) transition. We provide a microscopic model realization of this transition on the square lattice consisting of Heisenberg exchange (J_H) and biquadratic exchange (J_B) that favor a Néel phase, and a designed Q -term (Q_B) interaction which favors a cVBS through large-scale quantum Monte Carlo (QMC) simulations. For $J_H = 0$, this model is equivalent to the $SU(3)$ JQ model with a Néel-cVBS transition that has been argued to be DQC through QMC. Upon turning on J_H which brings down the symmetry to $SU(2)$, we find multiple signatures – a single critical point, high quality collapse of correlation ratios and order parameters, “ $U(1)$ -symmetric” cVBS histograms and lack of double-peak in order parameter histograms for largest sizes studied near the critical point – that are highly suggestive of a continuous transition scenario. However, Binder analysis finds negative dips that grow sub-extensively that we interpret as these transitions rather being pseudocritical. This along with recent results on spin- $\frac{1}{2}$ models suggests that deconfined pseudocriticality is the more generic scenario.

The theory of deconfined quantum criticality (DQC) has been of great interest since its inception [1–3] because it proposes a concrete theoretical scenario of a phase transition that is beyond the Landau-Ginzburg-Wilson paradigm. A continuous transition between two symmetry unrelated phases – Néel and VBS – was posited for spin- $\frac{1}{2}$ degrees of freedom in $2 + 1d$. Numerical hints of such a transition were seen in an earlier work [4]. The Berry phase interference effects [5–8] of the quantum degrees of freedom is crucial for the beyond-LGW nature. DQC is often described in terms of a gauge theory of fractionalized spinon degrees of freedom that deconfine only at the critical point. The Higgs condensation of the spinons leads to antiferromagnetic Néel order on one side, while on the other side the confinement of the associated $U(1)$ gauge field leads to valence bond crystallization. Given its appeal, it has subsequently undergone a great deal of scrutiny in various spin-1/2 models [9–20] and their $SU(N)$ generalizations [21–26], e.g. see the review [27]. Evidence for many proposed features of DQC have been numerically seen at the transition in these studies, including classical loop models and dimer models in $3d$ [28–31], certain $1d$ spin- $\frac{1}{2}$ extensions [32, 33], and fermionic models [34–38] argued to be in the same universality class. The issue is contentious though due to the various scaling violations observed [39–45], the origins of which are still being debated. Not much is however known for higher spins owing both to the emphasis of the original proposal and to the available recipes for constructing numerically accessible spin models that could host this physics [15].

In this work, our focus will be on spin-1 for which there are only a handful of papers discussing possible DQC and none which have shown DQC behavior in a microscopic model. In Ref. 46, Grover and Senthil pointed out the possibility of a DQC from a spin-nematic state

to a VBS state based on analogous field-theoretic arguments as in Ref. 2. In a later work [47], Wang, Kivelson and Lee proposed a possible DQC from a Néel state to a bond-nematic or Haldane-nematic state that may be caricatured as a symmetry broken stack of AKLT chains. They further conjectured possible DQC between a Néel to a cVBS state as a “doubled” version of the spin- $\frac{1}{2}$ DQC theory [48]. We are motivated to investigate this latter scenario due to the heuristic explained below.

The class of JQ models originated by Sandvik [9] have been crucial in probing DQC physics on bipartite lattices in large scale simulations. The basic units of these models are the singlet projectors $P_{ij} = (\frac{1}{4} - \mathbf{S}_i \cdot \mathbf{S}_j)$ on the bond $\langle ij \rangle$. A nice aspect of the projector formulation is that they can naturally be lifted [49] from $SU(2)$ to $SU(N)$ as $P_{ij} = \sum_{\alpha, \beta} |\alpha_i; \alpha_j\rangle \langle \beta_i; \beta_j|$. This has been exploited to study DQC in $N > 2$ microscopic models. The fluctuations of the $U(1)$ -gauge field get suppressed as N increases which makes for a closer match between perturbation theory estimates and numerical estimates of critical exponents [50]. For our purposes, we note that the $SU(3)$ JQ model can be recasted as a spin-1 model in terms of biquadratic exchanges due to an exact mapping between the $SU(3)$ singlet projector and the biquadratic exchange on a bond, $P_{ij} = \frac{1}{3} \{(\mathbf{S}_i \cdot \mathbf{S}_j)^2 - \mathbb{I}\}$ [21]. The $SU(3)$ JQ model was first studied by Lou, Sandvik and Kawashima in Ref. 22 where DQC behavior between Néel and VBS was observed for system sizes up to $L = 48$. As a spin-1 Hamiltonian, this maps to biquadratic exchange and a Q -term made out of them

$$H_{SU(3)} = -J_B \sum_{\langle ij \rangle} P_{ij} - Q_B \sum_{\langle ijkl \rangle} (P_{ij} P_{kl} + P_{il} P_{jk}) \quad (1)$$

where $\langle ijkl \rangle$ stands for an elementary plaquette of the square lattice with (say) a clockwise indexing of the sites on it. The first term favors Néel order. The Q -term

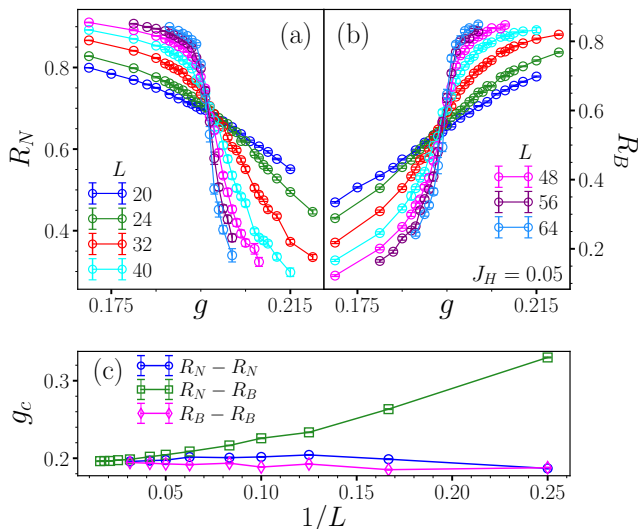


FIG. 1. Panels (a) and (b) shows respectively the correlation ratios of the Néel and cVBS order parameters (R_N and R_V) as described in the text ($g = Q_B/J_B$, $J_H = 0.05$, $\beta = \frac{L}{4}$). (c) shows g at the crossing of L and $L/2$ of R_N and R_V as an estimate of critical point ($g_c(L)$) versus $1/L$. The value of g at which R_N and R_V cross each other is also plotted here. The three ways of estimating the $g_c(L)$ converge to $g_c \sim 0.195$ implying a direct transition without an intermediate phase.

favors a cVBS of spin-1 valence bonds (which are also $SU(3)$ singlets for Eq. 1).

Here, we add an $SU(2)$ -symmetric perturbation in the form of the spin-1 Heisenberg exchange which also favors Néel order to study the same transition, i.e.

$$H_{SU(2)} = H_{SU(3)} + J_H \sum_{\langle ij \rangle} \{\mathbf{S}_i \cdot \mathbf{S}_j - \mathbb{I}\} \quad (2)$$

We study the Néel-cVBS quantum phase transition by varying $g \equiv \frac{Q_B}{J_B}$ for different values of J_H . With the recent introduction of new designer spin models for $S > 1/2$ systems [51], the above model has been rendered simulatable with the same powerful deterministic non-local loop updates as in the standard stochastic series expansion based finite-temperature QMC [52–54] for $S = 1/2$ models. Briefly, this is achieved by working in an expanded Hilbert space of two “split $S = \frac{1}{2}$ ”s per site with the addition of only one non-deterministic loop move at a single “projection” time slice to implement symmetrization over the two split $S = \frac{1}{2}$ s for all sites that restricts us to the physical $S = 1$ subspace [55, 56] in the QMC ensemble. An earlier work [57] had instead studied the $J_B = 0$ case and found strong first-order behavior. Thus, we will focus on the vicinity of $H_{SU(3)}$ as specified in Eq. 2 using standard notation (i refers to sites, $\langle ij \rangle$ refers to nearest neighbor bonds, \mathbf{S}_i refers to spin-1 operators on site i). We work in the units where $J_B = 1.0$. In presence of the $SU(2)$ -symmetric perturbation, the following scenarios may be expected: (1) $SU(3)$ criticality becomes

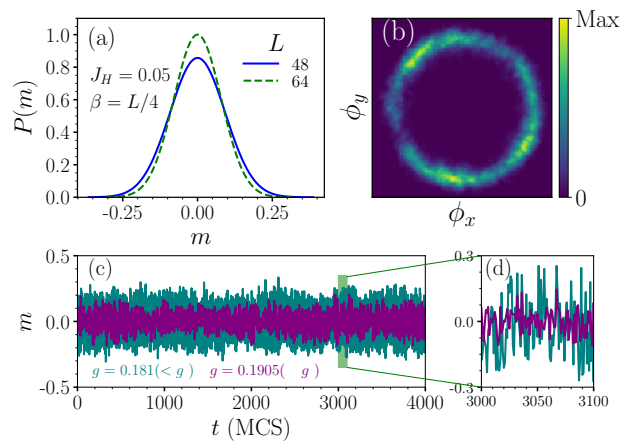


FIG. 2. (a) Histogram of staggered magnetization m (chosen along z -direction) for $J_H = 0.04$ near $g_c \sim 0.19$. (b) Heat Map of the cVBS order parameters (ϕ_x, ϕ_y) shows “ $U(1)$ -symmetric” nature characteristic of DQC. (c) The time series plot for m does not show any telegraphic switching behaviour ruling out a strong first-order transition. $L = 64$ in (b),(c).

first-order right upon turning on J_H and we see some cross-over physics for small values of the perturbation, (2) there is a regime of J_H for which the doubled $S = 1/2$ DQC scenario obtains, or (3) there is weakly first-order or pseudocritical behaviour in this regime. For the second scenario, we expect to see stable exponents that are either $SU(3)$ exponents or a new set of $SU(2)$ exponents in this regime.

We probe the system by measuring intensive order parameters for the two phases. For the Néel phase, the staggered magnetization order parameter $O_N \equiv \langle m^2 \rangle$, where $m = \frac{1}{N} \sum_{\mathbf{r}} e^{i(\pi, \pi) \cdot \mathbf{r}} S_{\mathbf{r}}^z$. For the columnar VBS phase, the cVBS order parameter $O_V \equiv \langle (\phi_x^2 + \phi_y^2) \rangle$, where $\phi_\mu = \frac{1}{N} \sum_{\mathbf{r}} e^{i\pi \mathbf{e}_\mu \cdot \mathbf{r}} \{(\mathbf{S}_{\mathbf{r}} \cdot \mathbf{S}_{\mathbf{r}+\mathbf{e}_\mu})^2 - \mathbb{I}\} / 3$ [59]. Throughout, the inverse temperature is set as $\beta = \frac{L}{4}$ to study ground state properties [60]. Correlation ratios of these order parameters [61] are plotted as a function of the coupling $g = \frac{Q_B}{J_B}$ in Fig 1. The ratios plotted for different system sizes show a crossing at the transition as shown for a representative value of J_H in Fig. 1a,b. The crossing points of both the Néel and VBS ratios converge as a function of $1/L$ (Fig. 1c) indicating a direct transition between the two phases with no intermediate phase.

Having established a direct transition, we now take a look at histograms of the order parameters to probe the nature of the transition. No signature of two-peak behavior in the histograms of the order parameters near the transition is seen as shown for staggered magnetization in Fig 2a. The characteristic telegraphic switching between the two order parameters at a first order transition is also absent near the transition (Fig 2c). This rules out the first scenario of a strongly first-order transition. Furthermore, “ $U(1)$ -symmetric” (ϕ_x, ϕ_y) -histograms are

TABLE I. Critical exponents (η_V, η_N, ν) as obtained from scaling collapse analysis of the order parameters ($O_{N,B}$) for different J_H . System sizes used for this analysis are in the range of $L = 24, 32, 40, 48, 64$. Additional corroborating analysis of correlation ratios and order parameters are shown in the Ref. [58].

| J_H | ν_N | ν_V | η_N | η_V | g_{cN} | g_{cV} | χ_N^2 | χ_V^2 |
|-------|---------|---------|----------|----------|----------|----------|------------|------------|
| 0.0 | 0.53(3) | 0.63(1) | 0.44(5) | 0.49(2) | 0.168(1) | 0.167(1) | 1.08-1.68 | 1.69-2.46 |
| 0.01 | 0.45(2) | 0.54(3) | 0.23(3) | 0.42(4) | 0.174(1) | 0.171(1) | 1.19-1.63 | 1.38-1.73 |
| 0.025 | 0.43(3) | 0.46(4) | 0.15(9) | 0.38(2) | 0.182(1) | 0.180(1) | 0.75-1.46 | 0.8-1.4 |
| 0.04 | 0.40(2) | 0.43(5) | 0.13(7) | 0.30(8) | 0.19(1) | 0.189(1) | 1.06-1.67 | 1.09-1.5 |
| 0.05 | 0.39(4) | 0.38(5) | 0.20(9) | 0.29(6) | 0.196(1) | 0.195(1) | 0.87-1.31 | 0.87-1.96 |
| 0.07 | 0.38(2) | 0.39(3) | 0.10(4) | 0.10(4) | 0.207(1) | 0.206(1) | 1.52-2.54 | 1.04-1.77 |
| 0.1 | 0.35(4) | 0.35(3) | -0.03(5) | -0.03(2) | 0.224(1) | 0.224(1) | 1.24-3.28 | 0.99-1.97 |
| 0.15 | 0.33(2) | 0.33(1) | 0.00(8) | -0.12(8) | 0.253(1) | 0.253(1) | 1.42-1.79 | 1.15-1.63 |

also seen near the transition for the largest system size studied (Fig 2b). In $S = \frac{1}{2}$ studies, this has been considered a key evidence of DQC. This is associated with the dangerous irrelevancy of the the operators in the DQC theory that capture the dominant quantum fluctuations during the transition out of the Néel phase. In our $S = 1$ model, the appropriate operators will be those of the doubled-DQC theory [62]. We therefore perform scaling collapses of the order parameters and the correlation ratios as shown in Fig. 3. The scaling collapses are of high quality throughout with the χ^2 per degree of freedom being close to 1 for all value of J_H studied. The exponents extracted from these finite-size scaling analysis are summarized in Table I. We find the exponents to be stable to various protocols involving the range of the tuning parameter g and system sizes used for the collapse analysis.

The first thing of note is that the anomalous exponents η_N and η_V are markedly different as soon as $J_H \neq 0$. For $J_H = 0$, we obtain $SU(3)$ exponents in overall agreement with earlier work of Lou *et al* [22] though our best estimate for the Néel correlation exponent ν_N is different. The collapse quality when ν_N is set same as ν_V (~ 0.63) is not significantly worse. The equality $\nu_N = \nu_V$ is one of the expectations in the theory of DQC. This marked difference from $J_H = 0$ suggests that $SU(3)$ criticality is not obtained when $J_H \neq 0$, i.e. the $SU(2)$ perturbation changes the universality class. This is not entirely unexpected and can be taken as evidence for the doubled spin-1/2 DQC scenario of Wang *et al* [47]. However, there is a slow drift in the exponents as J_H increases which argues against a stable set of exponents [63] as expected in the second scenario. The drift is noticeable even within the accuracy levels in the exponent estimates achieved by us. This level of accuracy in the estimation of critical exponents is not unusual in numerical studies of DQC. Similarly, the best estimates of ν_N and ν_V for each value of J_H do not match in all cases, but again setting them equal does not lead to significant loss of collapse quality similar to $J_H = 0$. Nevertheless, we certainly see that the anomalous exponents η_N, η_V are not small. This is one of the expectations in the theory of DQC which is strikingly

different than conventional second-order critical points, and seen in previous $S = \frac{1}{2}$ studies. Eventually, for large enough $J_H = 0.1$ and 0.15 , the anomalous exponents go negative indicating first-order behavior. This is to be expected since first-order behaviour has been seen for $J_B = 0$ [57], i.e. when J_H becomes large enough. The finite-size scaling analysis was performed using the Bayesian scheme implemented by Harada [64].

From the preceding discussions, the Néel-cVBS transition in Eq. 2 appears continuous up to $J_H \sim 0.07$. However, due to the observed drifts in the exponents, we further examine the Binder ratios of the magnetization order

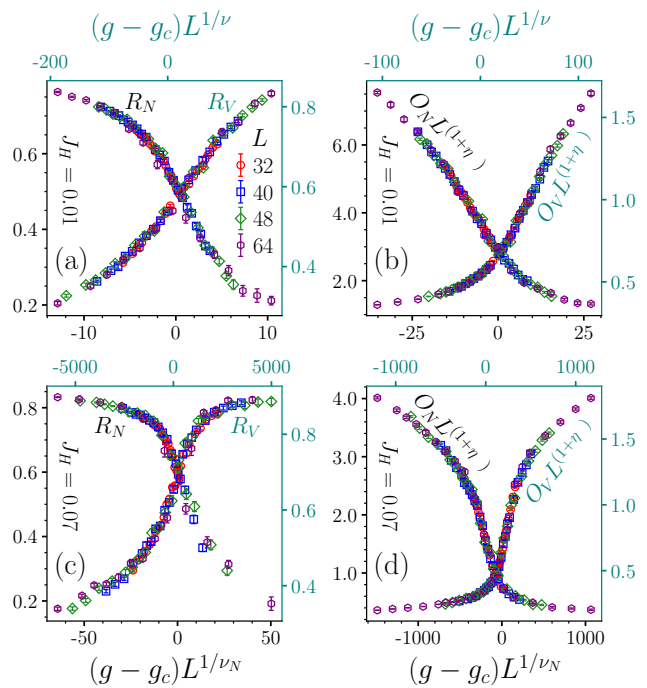


FIG. 3. Shown are scaling collapse of correlation ratios (R_N, R_V) and order parameters (O_N, O_V) for $J_H = 0.01$ and 0.07 with best estimates of the critical exponents (Table I). ($\beta = \frac{L}{4}$). Note the high quality of collapse as also seen through the χ^2 values in Table I that highly suggests a continuous transition within the doubled-DQC framework.

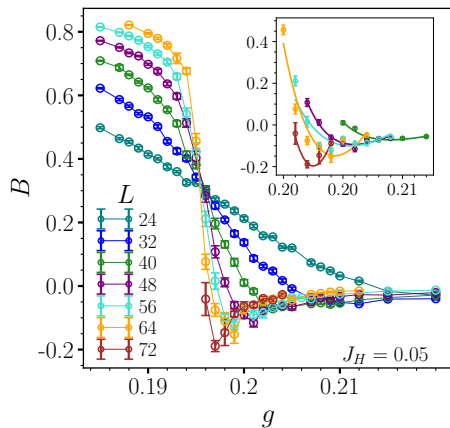


FIG. 4. Binder ratio plotted versus fugacity $g = Q_B/J_B$ for $J_H = 0.05$ ($\beta = \frac{L}{4}$). Similar plots with negative dips are obtained for other J_H values [58] as well which calls into question the continuous nature of the transition. The inset shows interpolations done in the vicinity of the Binder dip to extract an estimate of the dip magnitude versus L for Fig. 5.

parameter across this transition whose behavior would be expected to be similar to the correlation ratios. Fig 4 shows this ratio, defined as $\frac{5}{2}(3 - \frac{\langle m^4 \rangle}{\langle m^2 \rangle^2})$, with a clearly visible crossing at the transition point. Equally noteworthy is the clear dip below zero near the transition. This is seen for all values of J_H [58]. A characteristic of first order transitions is that this dip grows extensively as the system size. In Ref [41], where the $J_H = 0$ case was studied in the $SU(3)$ language, Kaul had noted that this dip grows subextensively as system size and interpreted it as evidence for a continuous transition. We similarly find that this negative dip grows slower than extensive in the regime of small J_H as shown in Fig 5. As J_H grows larger, it eventually grows as L^2 as expected for a first order transition [65, 66].

Given the lack of stability of the exponents seen earlier that would be expected for a bonafide DQC scenario, we rather interpret the subextensive growth of the Binder dip near the transition as evidence for deconfined pseudocriticality. In other words, the scenario of a doubled $S = \frac{1}{2}$ DQC provides a natural framework to understand the above set of numerical results, but the spinons get weakly confined at much larger length scales (dependent on J_H) than the lattice scale leading to the observed pseudocritical behavior as discussed more below. In terms of our simulations, we may imagine it as pseudo-DQC ensembles occurring in both the split $S = \frac{1}{2}$ Hilbert spaces in (QMC) space-time which then gets “inherited” by the $S = 1$ system under projection back to the fully symmetric subspace. This also implies a revision of the earlier interpretation of DQC in $SU(3)$ JQ model [41].

We conclude by situating our interpretation of deconfined pseudocriticality in our $S = 1$ microscopic model in the light of recent developments that have thrown

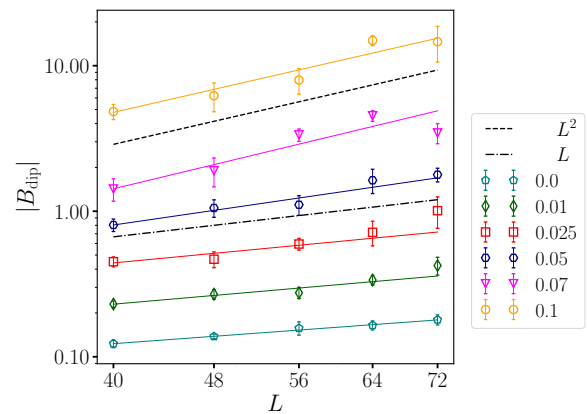


FIG. 5. (Negative) Binder dip magnitude versus L for different J_H . It scales subextensively for small J_H which we interpret as evidence for deconfined pseudocriticality in our $S = 1$ model. The dashed lines are L and (extensive) L^2 power laws, and the different J_H curves have been scaled by different constant factors for clarity of presentation.

open the issue of the putative second-order nature of DQCs [67–69]. These arose in the context of earlier works regarding emergent symmetry expectations at these transitions when interpreted in a $SO(5)$ framework with a combined order parameter built out of the Néel and VBS order parameters. The original $S = \frac{1}{2}$ DQC proposal can be re-expressed in terms of this combined order parameter with a single relevant perturbation tuning us across the transition [70, 71], which also implies an enhanced emergent symmetry between the two symmetry unrelated order parameters. This basic expectation has been numerically studied in various cases [45, 72], in certain unconventional transitions [73] including in one dimension [74, 75] and classical dimer models [76]. System size restrictions however makes interpretation of emergent symmetry tricky. From the theory side, conformal bootstrap results by Nakayama and Ohtsuki [77] pointed out strong constraints on the scaling dimensions that apparently rule out emergent symmetry in $2 + 1d$ DQC. Recent quantum entanglement based results by Diao *et al* [68] and Song *et al* [69] have significantly taken forward this line of argument. Ma, Wang [78], and Nahum [79] had thus conjectured the notion of DQC as pseudocriticality in order to reconcile with the conformal bootstrap result. The idea is that the RG fixed point for DQC does not reside in the (physical) $2 + 1d$, but slightly below it (see Fig. 1 of Ref. [78]) such that pseudocritically slow flows obtain near the critical point g_c . For a more detailed discussion on these issues, see this recent review [80]. Such slow RG flows may account for the good scaling collapse seen in numerical data for accessible system sizes *along* with the observed drifts in the critical exponents.

It is noteworthy that even before the emergent sym-

metry point of view gained currency, numerical studies of DQC had seen anomalous corrections to scalings whose origin was unclear. Bartosch gave an explanation based on scaling corrections inherent in the effective $U(1)$ gauge theory of the deconfined spinons [43]. A more recent explanation based on two different diverging length scales associated with spinon correlations and VBS domain wall sizes being governed by different exponents has been proposed by Shao, Guo and Sandvik as another possible resolution [44]. In the context of our interpretation, pseudocriticality rather implies the confinement of the spinons of the $U(1)$ gauge theory framework for all values of the tuning parameter, and the confinement length scale becomes very large ($L \gtrsim O(100)$ given the high quality of scaling collapses seen) compared the lattice scale [81] when the RG flow is pseudocritically slow near the apparent transition. The present consensus seems to be veering towards deconfined pseudocriticality based on recent $S = \frac{1}{2}$ results, and our work provides a microscopic $S = 1$ model for this scenario as yet not seen in the literature. This opens a mystery in the context of $SU(N)$ DQC where, on one hand, theoretical expectations based on the suppression of gauge fluctuations with increasing N make the case for bonafide DQC, but on the other hand, no negative Binder dips has been numerically seen in $SU(2)$ JQ models for largest sizes studied making the pattern of Binder dip growth with respect to N non-monotonic [82]. It will indeed be an useful theoretical advance and strong evidence for the pseudocriticality scenario if the subextensive growth of negative Binder ratio dips can be shown to be a generic consequence of the pseudocritical RG flows of Refs. [78, 79] that may further clarify the present state of affairs [69].

Acknowledgements:— We acknowledge useful discussions with Fabien Alet, Subhro Bhattacharjee, Kedar Damle, Prashant Kumar and Adam Nahum. VVi was supported by the institute post-doctoral fellowship program at IIT Bombay, and in part by the International Centre for Theoretical Sciences (ICTS) during the program - 8th Indian Statistical Physics Community Meeting (code: ICTS/ISPCM2023/02). SP acknowledges funding support from SERB-DST, India via Grants No. SRG/2019/001419 and MTR/2022/000386. Partial support by Grant No. CRG/2021/003024 is also acknowledged. ND was initially supported by National Postdoctoral Fellowship of SERB, DST, Govt. of India (PDF/2020/001658) at the department of Theoretical Physics, TIFR and presently by the TIFR postdoctoral fellowship. The numerical results were obtained using the computational facilities of the Department of Physics, Indian Institute of Technology (IIT) Bombay.

- [1] T. Senthil, A. Vishwanath, L. Balents, S. Sachdev, and M. P. A. Fisher, *Science* **303**, 1490 (2004), <https://www.science.org/doi/pdf/10.1126/science.1091806>, URL <https://www.science.org/doi/abs/10.1126/science.1091806>.
- [2] T. Senthil, L. Balents, S. Sachdev, A. Vishwanath, and M. P. A. Fisher, *Phys. Rev. B* **70**, 144407 (2004), URL <https://link.aps.org/doi/10.1103/PhysRevB.70.144407>.
- [3] M. Levin and T. Senthil, *Phys. Rev. B* **70**, 220403 (2004), URL <https://link.aps.org/doi/10.1103/PhysRevB.70.220403>.
- [4] A. W. Sandvik, S. Daul, R. R. P. Singh, and D. J. Scalapino, *Phys. Rev. Lett.* **89**, 247201 (2002), URL <https://link.aps.org/doi/10.1103/PhysRevLett.89.247201>.
- [5] N. Read and S. Sachdev, *Phys. Rev. Lett.* **62**, 1694 (1989), URL <https://link.aps.org/doi/10.1103/PhysRevLett.62.1694>.
- [6] N. Read and S. Sachdev, *Phys. Rev. B* **42**, 4568 (1990), URL <https://link.aps.org/doi/10.1103/PhysRevB.42.4568>.
- [7] N. Read and S. Sachdev, *Nuclear Physics B* **316**, 609 (1989), ISSN 0550-3213, URL <https://www.sciencedirect.com/science/article/pii/0550321389900618>.
- [8] F. D. M. Haldane, *Phys. Rev. Lett.* **61**, 1029 (1988), URL <https://link.aps.org/doi/10.1103/PhysRevLett.61.1029>.
- [9] A. W. Sandvik, *Phys. Rev. Lett.* **98**, 227202 (2007), URL <http://link.aps.org/doi/10.1103/PhysRevLett.98.227202>.
- [10] R. G. Melko and R. K. Kaul, *Phys. Rev. Lett.* **100**, 017203 (2008), URL <https://link.aps.org/doi/10.1103/PhysRevLett.100.017203>.
- [11] A. W. Sandvik, *Phys. Rev. Lett.* **104**, 177201 (2010), URL <https://link.aps.org/doi/10.1103/PhysRevLett.104.177201>.
- [12] A. Banerjee, K. Damle, and F. Alet, *Phys. Rev. B* **82**, 155139 (2010), URL <https://link.aps.org/doi/10.1103/PhysRevB.82.155139>.
- [13] A. Banerjee, K. Damle, and F. Alet, *Phys. Rev. B* **83**, 235111 (2011), URL <https://link.aps.org/doi/10.1103/PhysRevB.83.235111>.
- [14] A. W. Sandvik, *Phys. Rev. B* **85**, 134407 (2012), URL <https://link.aps.org/doi/10.1103/PhysRevB.85.134407>.
- [15] R. K. Kaul, *Phys. Rev. B* **91**, 54413 (2015), URL <http://link.aps.org/doi/10.1103/PhysRevB.91.054413>.
- [16] S. Pujari, K. Damle, and F. Alet, *Phys. Rev. Lett.* **111**, 087203 (2013), URL <https://link.aps.org/doi/10.1103/PhysRevLett.111.087203>.
- [17] S. Pujari, F. Alet, and K. Damle, *Phys. Rev. B* **91**, 104411 (2015), URL <https://link.aps.org/doi/10.1103/PhysRevB.91.104411>.
- [18] N. Ma, Y.-Z. You, and Z. Y. Meng, *Phys. Rev. Lett.* **122**, 175701 (2019), URL <https://link.aps.org/doi/10.1103/PhysRevLett.122.175701>.
- [19] B. Zhao, J. Takahashi, and A. W. Sandvik, *Phys. Rev. Lett.* **125**, 257204 (2020), URL <https://link.aps.org/doi/10.1103/PhysRevLett.125.257204>.
- [20] A. W. Sandvik and B. Zhao, *Chinese Physics Letters* **37**, 057502 (2020), URL <https://dx.doi.org/10.1088/0256-307X/37/5/057502>.

* sumiran.pujari@iitb.ac.in

- [21] K. S. D. Beach, F. Alet, M. Mambrini, and S. Capponi, Phys. Rev. B **80**, 184401 (2009), URL <https://link.aps.org/doi/10.1103/PhysRevB.80.184401>.
- [22] J. Lou, A. W. Sandvik, and N. Kawashima, Phys. Rev. B **80**, 180414 (2009), URL <https://link.aps.org/doi/10.1103/PhysRevB.80.180414>.
- [23] R. K. Kaul, Phys. Rev. B **85**, 180411 (2012), URL <https://link.aps.org/doi/10.1103/PhysRevB.85.180411>.
- [24] R. K. Kaul and A. W. Sandvik, Phys. Rev. Lett. **108**, 137201 (2012), URL <https://link.aps.org/doi/10.1103/PhysRevLett.108.137201>.
- [25] M. S. Block, R. G. Melko, and R. K. Kaul, Phys. Rev. Lett. **111**, 137202 (2013), URL <https://link.aps.org/doi/10.1103/PhysRevLett.111.137202>.
- [26] K. Harada, T. Suzuki, T. Okubo, H. Matsuo, J. Lou, H. Watanabe, S. Todo, and N. Kawashima, Phys. Rev. B **88**, 220408 (2013), URL <https://link.aps.org/doi/10.1103/PhysRevB.88.220408>.
- [27] R. K. Kaul, R. G. Melko, and A. W. Sandvik, Annu. Rev. Cond. Matt. Phys **4**, 179 (2013), URL <http://www.annualreviews.org/doi/abs/10.1146/annurev-conmatphys-030212-184215>.
- [28] D. Charrier, F. Alet, and P. Pujol, Phys. Rev. Lett. **101**, 167205 (2008), URL <https://link.aps.org/doi/10.1103/PhysRevLett.101.167205>.
- [29] S. Powell and J. T. Chalker, Phys. Rev. Lett. **101**, 155702 (2008), URL <https://link.aps.org/doi/10.1103/PhysRevLett.101.155702>.
- [30] S. Powell and J. T. Chalker, Phys. Rev. B **80**, 134413 (2009), URL <https://link.aps.org/doi/10.1103/PhysRevB.80.134413>.
- [31] G. Chen, J. Gukelberger, S. Trebst, F. Alet, and L. Balents, Phys. Rev. B **80**, 045112 (2009), URL <https://link.aps.org/doi/10.1103/PhysRevB.80.045112>.
- [32] B. Roberts, S. Jiang, and O. I. Motrunich, Phys. Rev. B **99**, 165143 (2019), URL <https://link.aps.org/doi/10.1103/PhysRevB.99.165143>.
- [33] R.-Z. Huang, D.-C. Lu, Y.-Z. You, Z. Y. Meng, and T. Xiang, Phys. Rev. B **100**, 125137 (2019), URL <https://link.aps.org/doi/10.1103/PhysRevB.100.125137>.
- [34] Y. Da Liao, X. Y. Xu, Z. Y. Meng, and Y. Qi, Phys. Rev. B **106**, 075111 (2022), URL <https://link.aps.org/doi/10.1103/PhysRevB.106.075111>.
- [35] Y. Da Liao, X. Y. Xu, Z. Y. Meng, and Y. Qi, Phys. Rev. B **106**, 155159 (2022), URL <https://link.aps.org/doi/10.1103/PhysRevB.106.155159>.
- [36] T. Sato, M. Hohenadler, and F. F. Assaad, Phys. Rev. Lett. **119**, 197203 (2017), URL <https://link.aps.org/doi/10.1103/PhysRevLett.119.197203>.
- [37] Z.-X. Li, Y.-F. Jiang, S.-K. Jian, and H. Yao, Nature Communications **8**, 314 (2017), ISSN 2041-1723, URL <https://doi.org/10.1038/s41467-017-00167-6>.
- [38] Z.-X. Li, S.-K. Jian, and H. Yao, arXiv e-prints arXiv:1904.10975 (2019), 1904.10975.
- [39] A. Kuklov, N. Prokof'ev, B. Svistunov, and M. Troyer, Annals of Physics **321**, 1602 (2006), ISSN 0003-4916, July 2006 Special Issue, URL <https://www.sciencedirect.com/science/article/pii/S0003491606000789>.
- [40] F.-J. Jiang, M. Nyfeler, S. Chandrasekharan, and U.-J. Wiese, Journal of Statistical Mechanics: Theory and Experiment **2008**, P02009 (2008), URL <https://dx.doi.org/10.1088/1742-5468/2008/02/P02009>.
- [41] R. K. Kaul, Phys. Rev. B **84**, 054407 (2011), URL <https://link.aps.org/doi/10.1103/PhysRevB.84.054407>.
- [42] K. Chen, Y. Huang, Y. Deng, A. B. Kuklov, N. V. Prokof'ev, and B. V. Svistunov, Phys. Rev. Lett. **110**, 185701 (2013), URL <https://link.aps.org/doi/10.1103/PhysRevLett.110.185701>.
- [43] L. Bartosch, Phys. Rev. B **88**, 195140 (2013), URL <https://link.aps.org/doi/10.1103/PhysRevB.88.195140>.
- [44] H. Shao, W. Guo, and A. W. Sandvik, Science **352**, 213 (2016), <https://www.science.org/doi/pdf/10.1126/science.aad5007>, URL <https://www.science.org/doi/abs/10.1126/science.aad5007>.
- [45] A. Nahum, J. T. Chalker, P. Serna, M. Ortuño, and A. M. Somoza, Phys. Rev. X **5**, 041048 (2015), URL <https://link.aps.org/doi/10.1103/PhysRevX.5.041048>.
- [46] T. Grover and T. Senthil, Phys. Rev. Lett. **98**, 247202 (2007), URL <https://link.aps.org/doi/10.1103/PhysRevLett.98.247202>.
- [47] F. Wang, S. A. Kivelson, and D.-H. Lee, Nature Physics **11**, 959 (2015), ISSN 1745-2481, URL <https://doi.org/10.1038/nphys3456>.
- [48] See the supplementary information for Ref. [47]. The Néel-cVBS transition that we are focusing on is mentioned in point (i) of the itemized list at the bottom of page 4. Point (ii) of this list predicts first-order transitions between ferro-spin-nematic and cVBS and Hadlane-nematic states as opposed to the second-order examples mentioned in our paper.
- [49] The equality obtains after a well-known sublattice dependent unitary transformation, where on every “B”-sublattice site one performs 180° rotation about the y -axis and nothing (identity transformation) on the “A”-sublattice sites of a bipartite lattice.
- [50] See Fig. 5 of Ref 25.
- [51] N. Desai and R. K. Kaul, Phys. Rev. Lett. **123**, 107202 (2019), URL <https://link.aps.org/doi/10.1103/PhysRevLett.123.107202>.
- [52] A. W. Sandvik and J. Kurkijärvi, Phys. Rev. B **43**, 5950 (1991), URL <https://link.aps.org/doi/10.1103/PhysRevB.43.5950>.
- [53] A. W. Sandvik, Journal of Physics A: Mathematical and General **25**, 3667 (1992), URL <https://doi.org/10.1088/0305-4470/25/13/017>.
- [54] A. W. Sandvik, in *Lectures on the Physics of Strongly Correlated Systems Xiv: Fourteenth Training Course in the Physics of Strongly Correlated Systems*, edited by A. Avella and F. Mancini (2010), vol. 1297 of *American Institute of Physics Conference Series*, pp. 135–338, 1101.3281.
- [55] N. Kawashima and J. E. Gubernatis, Journal of Statistical Physics **80**, 169 (1995), ISSN 1572-9613, URL <https://doi.org/10.1007/BF02178358>.
- [56] S. Todo and K. Kato, Phys. Rev. Lett. **87**, 047203 (2001), URL <https://link.aps.org/doi/10.1103/PhysRevLett.87.047203>.
- [57] J. Wildeboer, N. Desai, J. D’Emidio, and R. K. Kaul, Phys. Rev. B **101**, 045111 (2020), URL <https://link.aps.org/doi/10.1103/PhysRevB.101.045111>.
- [58] See Supplemental Material at ... for further details.
- [59] Note we use the biquadratic exchange term to construct the cVBS order parameter instead of the more frequently used Heisenberg exchange term. Both constructions can probe cVBS order; our choice has better statistics in terms of QMC estimation for the parameter regime we

- are interested in, i.e. the vicinity of $J_H = 0$.
- [60] See Fig. I,II,III of supplemental document [58] for low-temperature convergence with respect to β .
- [61] These are calculated by taking the ratio of the Fourier transform of the correlation functions ($\tilde{C}(k)$) at the ordering momentum, k_o , and a momentum closest to it (in some chosen direction) at the given system size, $k_{o'}$, $R \equiv 1 - \frac{\tilde{C}(k_{o'})}{\tilde{C}(k_o)}$. It can be verified that $R \rightarrow 1$ and 0 as $L \rightarrow \infty$ in the ordered and disordered phases respectively.
- [62] Technically, these have been called as (quadrupled) monopole operators or, in terms of space-time, instantons. On the square lattice for $S = \frac{1}{2}$, they capture the tunneling events that changes the net skyrmion number of Néel order parameter field by multiples of four due to the particularities of the Berry phase terms [2, 8]. For our $S = 1$ model, we may imagine the same tunneling events occurring in both the split $S = \frac{1}{2}$ channels or layers in space-time which connects naturally to the doubled-DQC scenario of Ref. [47].
- [63] For an example of a stable set of exponents, see Table I of Ref. [17].
- [64] K. Harada, Phys. Rev. E **84**, 056704 (2011), URL <https://link.aps.org/doi/10.1103/PhysRevE.84.056704>.
- [65] K. Vollmayr, J. D. Reger, M. Scheucher, and K. Binder, Zeitschrift für Physik B Condensed Matter **91**, 113 (1993), ISSN 1431-584X, URL <https://doi.org/10.1007/BF01316713>.
- [66] A. Sen and A. W. Sandvik, Phys. Rev. B **82**, 174428 (2010), URL <https://link.aps.org/doi/10.1103/PhysRevB.82.174428>.
- [67] J. D'Emidio, A. A. Eberharter, and A. M. Läuchli, arXiv e-prints arXiv:2106.15462 (2021), 2106.15462.
- [68] Y. Da Liao, G. Pan, W. Jiang, Y. Qi, and Z. Y. Meng, arXiv e-prints arXiv:2302.11742 (2023), 2302.11742, URL <https://arxiv.org/abs/2302.11742>.
- [69] M. Song, J. Zhao, L. Janssen, M. M. Scherer, and Z. Y. Meng, *Deconfined quantum criticality lost* (2023), 2307.02547, URL <https://arxiv.org/abs/2307.02547>.
- [70] A. Tanaka and X. Hu, Phys. Rev. Lett. **95**, 036402 (2005), URL <https://link.aps.org/doi/10.1103/PhysRevLett.95.036402>.
- [71] T. Senthil and M. P. A. Fisher, Phys. Rev. B **74**, 064405 (2006), URL <https://link.aps.org/doi/10.1103/PhysRevB.74.064405>.
- [72] A. Nahum, P. Serna, J. T. Chalker, M. Ortuño, and A. M. Somoza, Phys. Rev. Lett. **115**, 267203 (2015), URL <https://link.aps.org/doi/10.1103/PhysRevLett.115.267203>.
- [73] B. Zhao, P. Weinberg, and A. W. Sandvik, Nature Physics **15**, 678 (2019), ISSN 1745-2481, URL <https://doi.org/10.1038/s41567-019-0484-x>.
- [74] P. Patil, E. Katz, and A. W. Sandvik, Phys. Rev. B **98**, 014414 (2018), URL <https://link.aps.org/doi/10.1103/PhysRevB.98.014414>.
- [75] N. Xi and R. Yu, Journal of Physics A: Mathematical and Theoretical **55**, 304003 (2022), URL <https://dx.doi.org/10.1088/1751-8121/ac7181>.
- [76] G. J. Sreejith, S. Powell, and A. Nahum, Phys. Rev. Lett. **122**, 080601 (2019), URL <https://link.aps.org/doi/10.1103/PhysRevLett.122.080601>.
- [77] Y. Nakayama and T. Ohtsuki, Phys. Rev. Lett. **117**, 131601 (2016), URL <https://link.aps.org/doi/10.1103/PhysRevLett.117.131601>.
- [78] R. Ma and C. Wang, Phys. Rev. B **102**, 020407 (2020), URL <https://link.aps.org/doi/10.1103/PhysRevB.102.020407>.
- [79] A. Nahum, Phys. Rev. B **102**, 201116 (2020), URL <https://link.aps.org/doi/10.1103/PhysRevB.102.201116>.
- [80] T. Senthil, *Deconfined quantum critical points: a review* (2023), 2306.12638.
- [81] A. Sandvik, *Vasp webinar at s.n. bose center for basic sciences, 2022*, URL https://www.youtube.com/watch?v=rg-WW2Z9_pg.
- [82] See Fig. 1 of Ref. [41] and associated discussion on the Binder dip magnitude in it.

Supplementary information for “Deconfined pseudocriticality in a model spin-1 quantum antiferromagnet”

Vikas Vijigiri,^{1,*} Nisheeta Desai,² and Sumiran Pujari^{1,†}

¹*Department of Physics, Indian Institute of Technology Bombay, Powai, Mumbai, 400076, India*

²*Department of Theoretical Physics, Tata Institute of Fundamental Research, Mumbai, 400005, India*

(Dated: July 27, 2023)

Here we present additional data and plots to document the data sets collected during this work for the various Heisenberg exchange coupling (J_H) values studied in the main text.

CONTENTS

| | |
|--|----|
| I. Model and Observables | 1 |
| II. Data sets | 3 |
| A. Convergence with inverse temperature β | 3 |
| B. Correlation Ratios | 6 |
| C. Staggered magnetization histograms | 8 |
| D. cVBS order parameter histograms | 9 |
| E. Staggered magnetization time series | 10 |
| F. cVBS order parameter time series | 12 |
| G. Scaling collapse of correlation ratios and order parameters | 15 |
| H. Binder Ratios | 17 |
| III. Tables | 18 |
| A. Critical exponents and critical point estimates | 18 |
| B. Benchmarking with Exact Diagonalization | 19 |

I. MODEL AND OBSERVABLES

We recapitulate again the various definitions related to the model and observables introduced in the main text for convenience. The $S = 1$ Hamiltonian (Eq. 1 and Eq. 2 of the main text) is given by,

$$\begin{aligned}
 H = & J_H \sum_{\langle ij \rangle} \{\mathbf{S}_i \cdot \mathbf{S}_j - \mathbb{I}\} - \frac{J_B}{3} \sum_{\langle ij \rangle} \{(\mathbf{S}_i \cdot \mathbf{S}_j)^2 - \mathbb{I}\} \\
 & - \frac{Q_B}{9} \sum_{\langle ijkl \rangle} [\{(\mathbf{S}_i \cdot \mathbf{S}_j)^2 - \mathbb{I}\}\{(\mathbf{S}_k \cdot \mathbf{S}_l)^2 - \mathbb{I}\} + \{(\mathbf{S}_i \cdot \mathbf{S}_l)^2 - \mathbb{I}\}\{(\mathbf{S}_j \cdot \mathbf{S}_k)^2 - \mathbb{I}\}]
 \end{aligned} \tag{1}$$

where J_H, J_B are the coefficients of the Heisenberg and Biquadratic exchange terms, and Q_B is the coefficient of the designer Q -term composed of biquadratic exchanges respectively.

* vikas.v@iitb.ac.in

† sumiran@phy.iitb.ac.in

The following structure factors

$$\mathcal{A}(\mathbf{q}) = \frac{1}{N^2} \sum_{\mathbf{r}, \mathbf{r}'} e^{i(\mathbf{r}-\mathbf{r}') \cdot \mathbf{q}} \langle S_{\mathbf{r}}^z S_{\mathbf{r}'}^z \rangle \quad (2)$$

$$\mathcal{B}(\mathbf{q}) = \frac{1}{N^2} \sum_{\mathbf{r}, \mathbf{r}'} e^{i(\mathbf{r}-\mathbf{r}') \cdot \mathbf{q}} \langle (\mathbf{S}_{\mathbf{r}} \cdot \mathbf{S}_{\mathbf{r}'} - \mathbb{I}) \rangle \quad (3)$$

$$\mathcal{C}^\mu(\mathbf{q}) = \frac{1}{N^2} \sum_{\mathbf{r}, \mathbf{r}'} e^{i(\mathbf{r}-\mathbf{r}') \cdot \mathbf{q}} \langle (\mathbf{S}_{\mathbf{r}} \cdot \mathbf{S}_{\mathbf{r}+\mathbf{e}_\mu} - \mathbb{I}) \times (\mathbf{S}_{\mathbf{r}'} \cdot \mathbf{S}_{\mathbf{r}'+\mathbf{e}_\mu} - \mathbb{I}) \rangle \quad (4)$$

$$\mathcal{D}^\mu(\mathbf{q}) = \frac{1}{9N^2} \sum_{\mathbf{r}, \mathbf{r}'} e^{i(\mathbf{r}-\mathbf{r}') \cdot \mathbf{q}} \langle ((\mathbf{S}_{\mathbf{r}} \cdot \mathbf{S}_{\mathbf{r}+\mathbf{e}_\mu})^2 - \mathbb{I}) \times ((\mathbf{S}_{\mathbf{r}'} \cdot \mathbf{S}_{\mathbf{r}'+\mathbf{e}_\mu})^2 - \mathbb{I}) \rangle \quad (5)$$

made out of real-space correlators can serve as order parameters for Néel and VBS ordering. As a side remark, $\mathcal{B}(\mathbf{q})$ can be measured during loop update in SSE. However, we do not need to do this as $\mathcal{A}(\mathbf{q})$ which also detects Néel ordering can be measured in a much simpler way. Furthermore, in presence of $SU(2)$ symmetry they are linearly related to each other. Therefore, we focused on $\mathcal{A}(\mathbf{q})$ to probe Néel order at the antiferromagnetic ordering wavevector on the square lattice ((π, π) when lattice constants are set to unity) as mentioned in the main text as well. The corresponding Néel correlation ratio R_N is defined to be

$$R_N \equiv \frac{R_x + R_y}{2} \quad (6)$$

where,

$$R_x \equiv 1 - \frac{\mathcal{A}(\pi + \frac{2\pi}{L}, \pi)}{\mathcal{A}(\pi, \pi)} \quad (7)$$

$$R_y \equiv 1 - \frac{\mathcal{A}(\pi, \pi + \frac{2\pi}{L})}{\mathcal{A}(\pi, \pi)} \quad (8)$$

Similarly, both $\mathcal{C}(\mathbf{q})$ and $\mathcal{D}(\mathbf{q})$ made out of bond-bond correlators of Heisenberg and biquadratic couplings can be used to probe VBS order at its ordering wavevector on the square lattice ($(\pi, 0)$ and $(0, \pi)$ when lattice constants are set to unity). Either one would thus suffice for the study of Néel-VBS transitions. The Heisenberg bond energy based VBS correlation ratio $R_{V'}$ is defined to be

$$R_{V'} \equiv \frac{R_{V'_x} + R_{V'_y}}{2} \quad (9)$$

where,

$$R_{V'_x} \equiv 1 - \frac{\mathcal{C}(\pi + \frac{2\pi}{L}, 0)}{\mathcal{C}(\pi, 0)} \quad (10)$$

$$R_{V'_y} \equiv 1 - \frac{\mathcal{C}(0, \pi + \frac{2\pi}{L})}{\mathcal{C}(0, \pi)} \quad (11)$$

We have rather focused on the biquadratic bond energy based VBS observables in the paper due to better statistics while estimating it during QMC compared to the Heisenberg bond energy based observables as discussed also in a footnote in the main text. The corresponding VBS correlation ratio is thus defined to

$$R_V \equiv \frac{R_{V_x} + R_{V_y}}{2} \quad (12)$$

where,

$$R_{V_x} = 1 - \frac{\mathcal{D}(\pi + \frac{2\pi}{L}, 0)}{\mathcal{D}(\pi, 0)} \quad (13)$$

$$R_{V_y} = 1 - \frac{\mathcal{D}(0, \pi + \frac{2\pi}{L})}{\mathcal{D}(0, \pi)} \quad (14)$$

Finally, from the above we can also see the correspondence between the notation of the main text and that used here for the order parameters as

$$O_N = \mathcal{A}(\pi, \pi) \quad (15)$$

$$O_V = \mathcal{D}^x(\pi, 0) + \mathcal{D}^y(0, \pi) \quad (16)$$

II. DATA SETS

A. Convergence with inverse temperature β

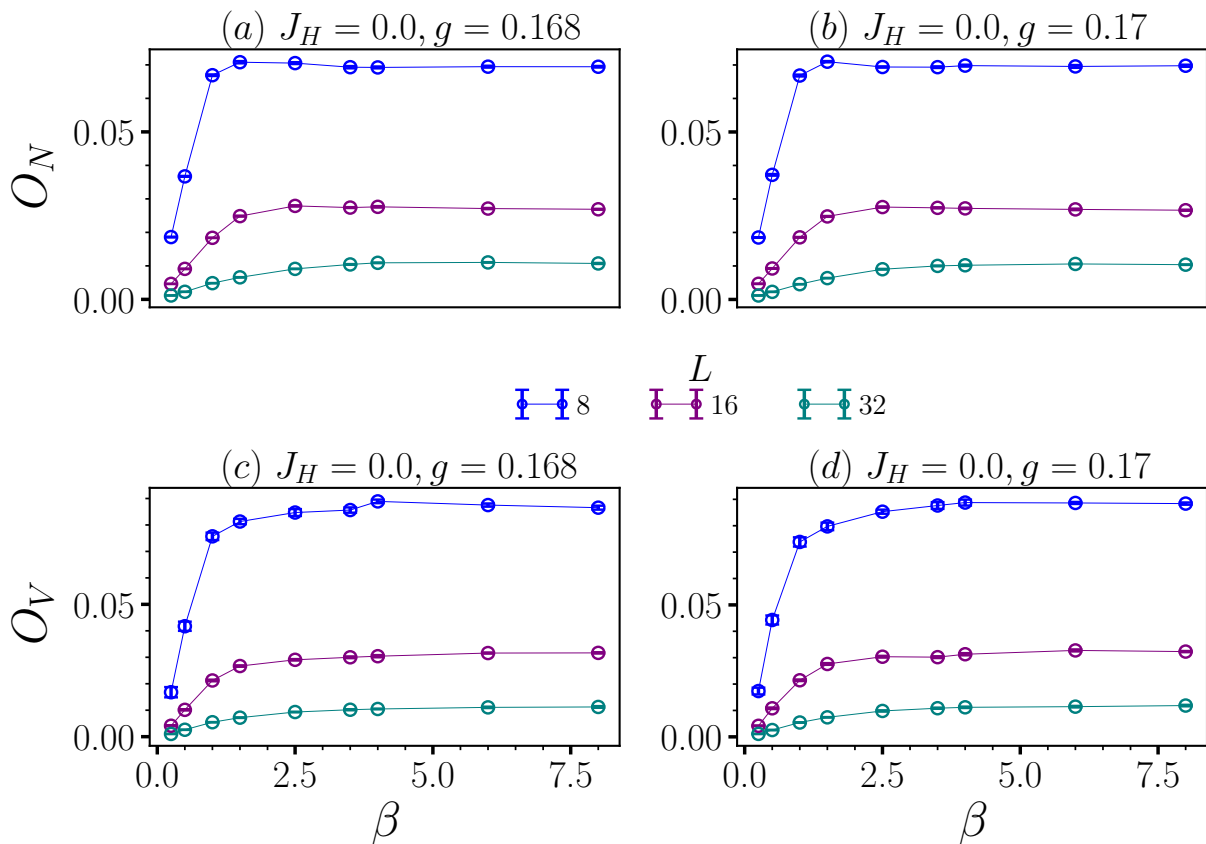


FIG. 1. Néel and cVBS order parameters (O_N and O_V) versus the inverse temperature $\beta = \frac{1}{T}$. $\frac{J_H}{J_B} = 0.0$, $g \equiv \frac{Q_B}{J_B} \sim 0.17$. We recall that J_B is set to 1 everywhere. Similar behaviour is present everywhere in the parameter regimes explored as illustrated through the next two figures. We see that $\beta = \frac{L}{4}$ is more than sufficient for making conclusions about ground state properties.

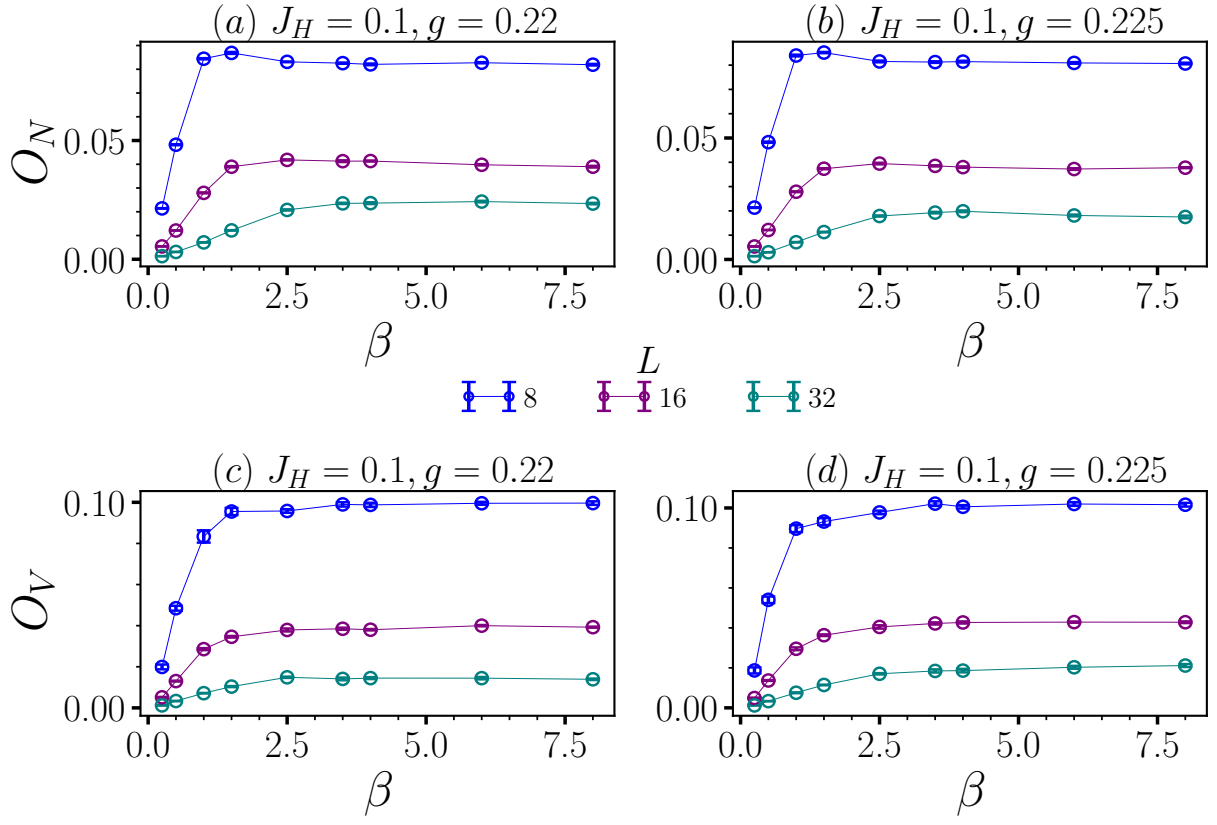


FIG. 2. Néel and cVBS order parameters (O_N and O_V) versus the inverse temperature $\beta = \frac{1}{T}$. $\frac{J_H}{J_B} = 0.1$, $g \equiv \frac{Q_B}{J_B} \sim 0.22$.

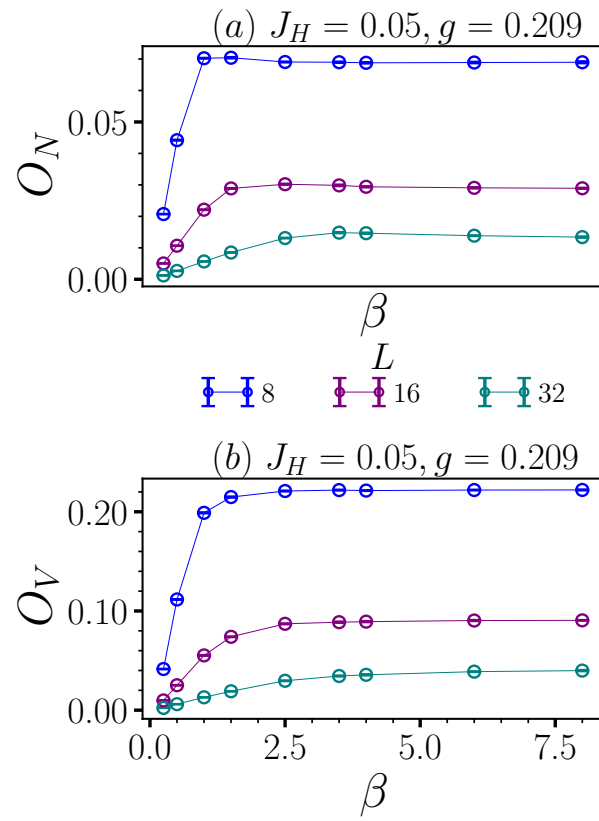


FIG. 3. Néel and cVBS order parameters (O_N and O_V) versus the inverse temperature $\beta = \frac{1}{T}$. $\frac{J_H}{J_B} = 0.0$, $g \equiv \frac{Q_B}{J_B} \sim 0.21$.

B. Correlation Ratios

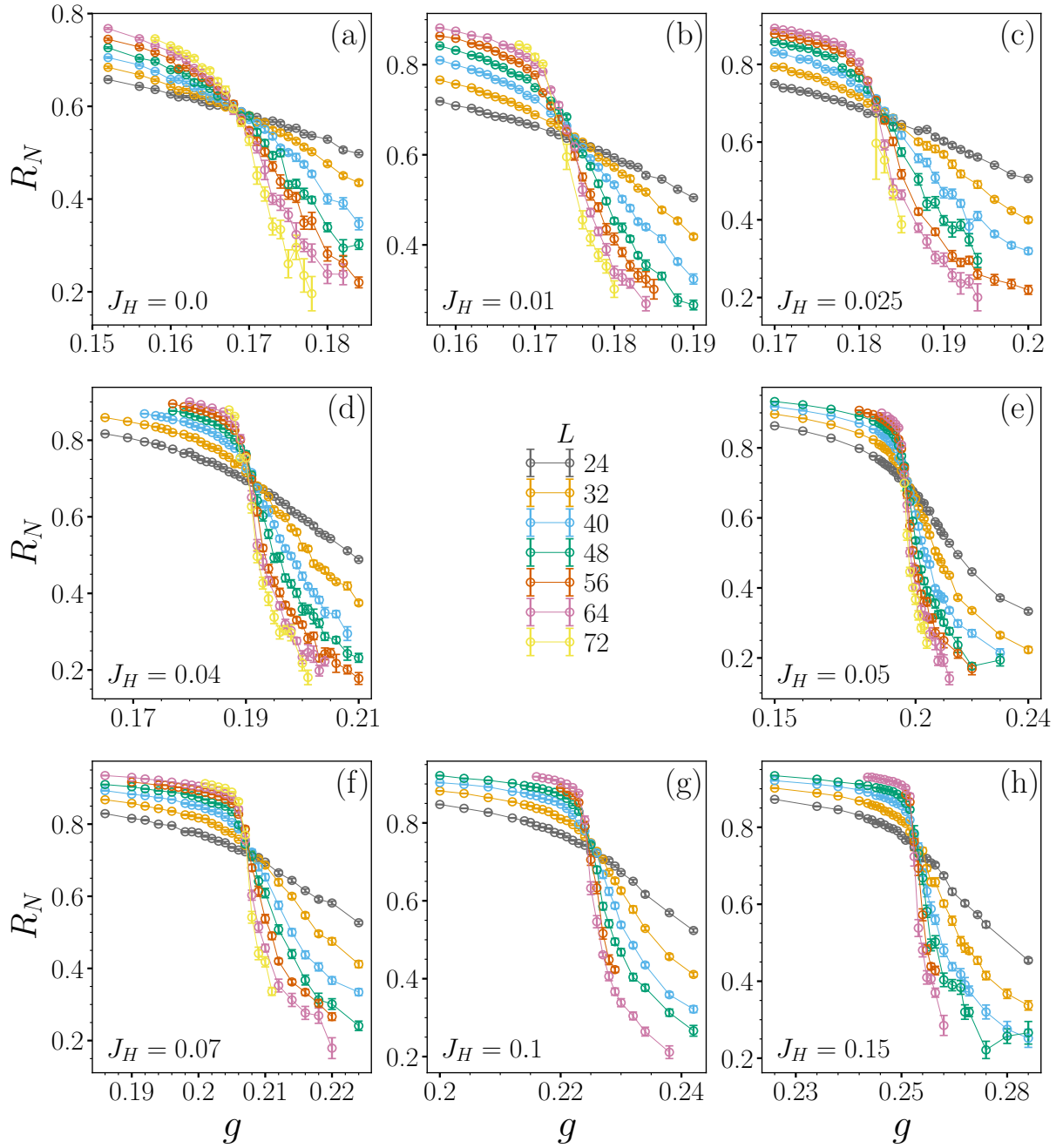


FIG. 4. This figure expands on Fig. 1a of the main text to document all the R_N correlation ratio data sets collected. $\beta = \frac{L}{4}$ throughout.

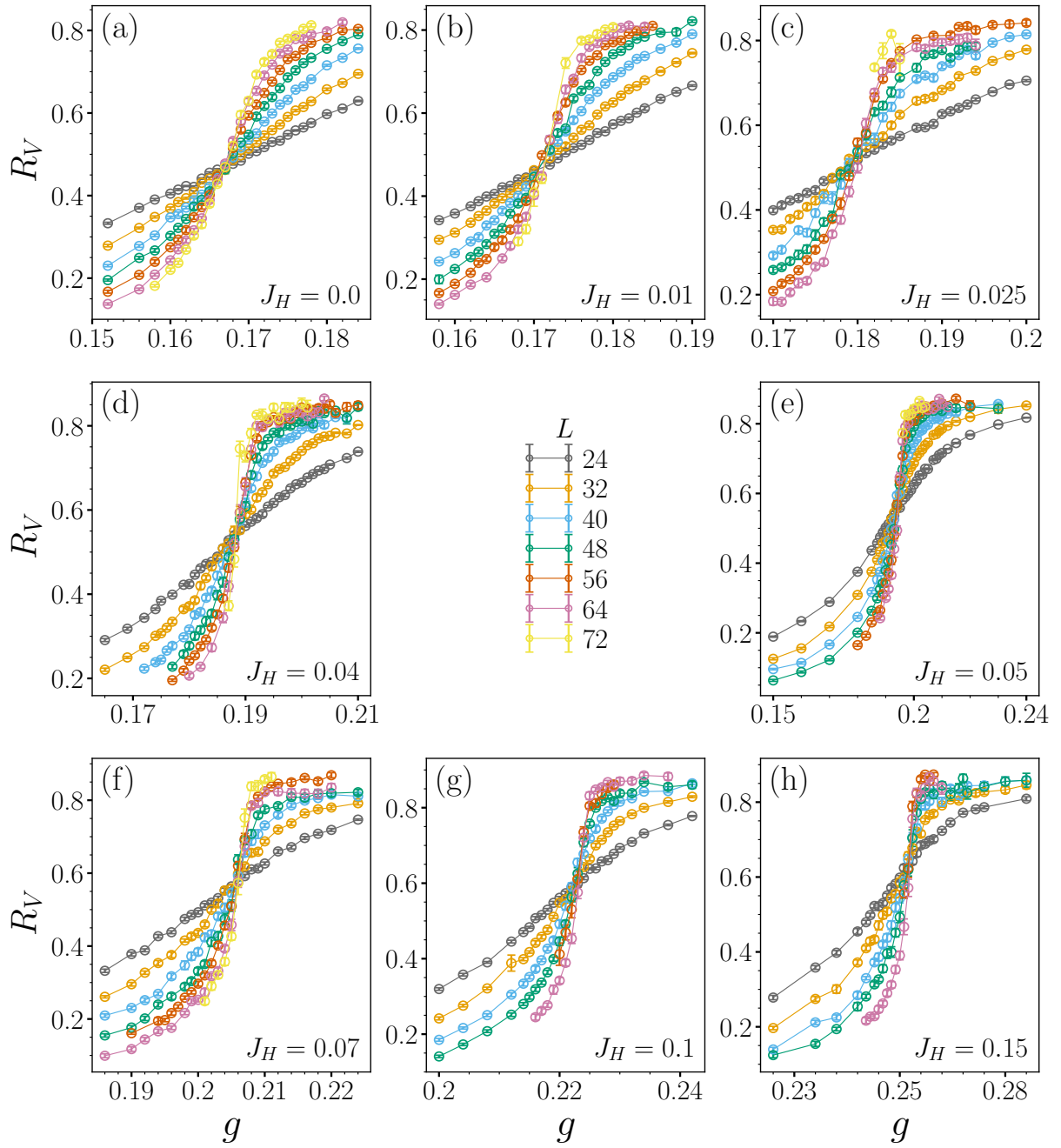


FIG. 5. This figure expands on Fig. 1b of the main text to document all the R_V correlation ratio data sets collected. $\beta = \frac{L}{4}$ throughout.

C. Staggered magnetization histograms

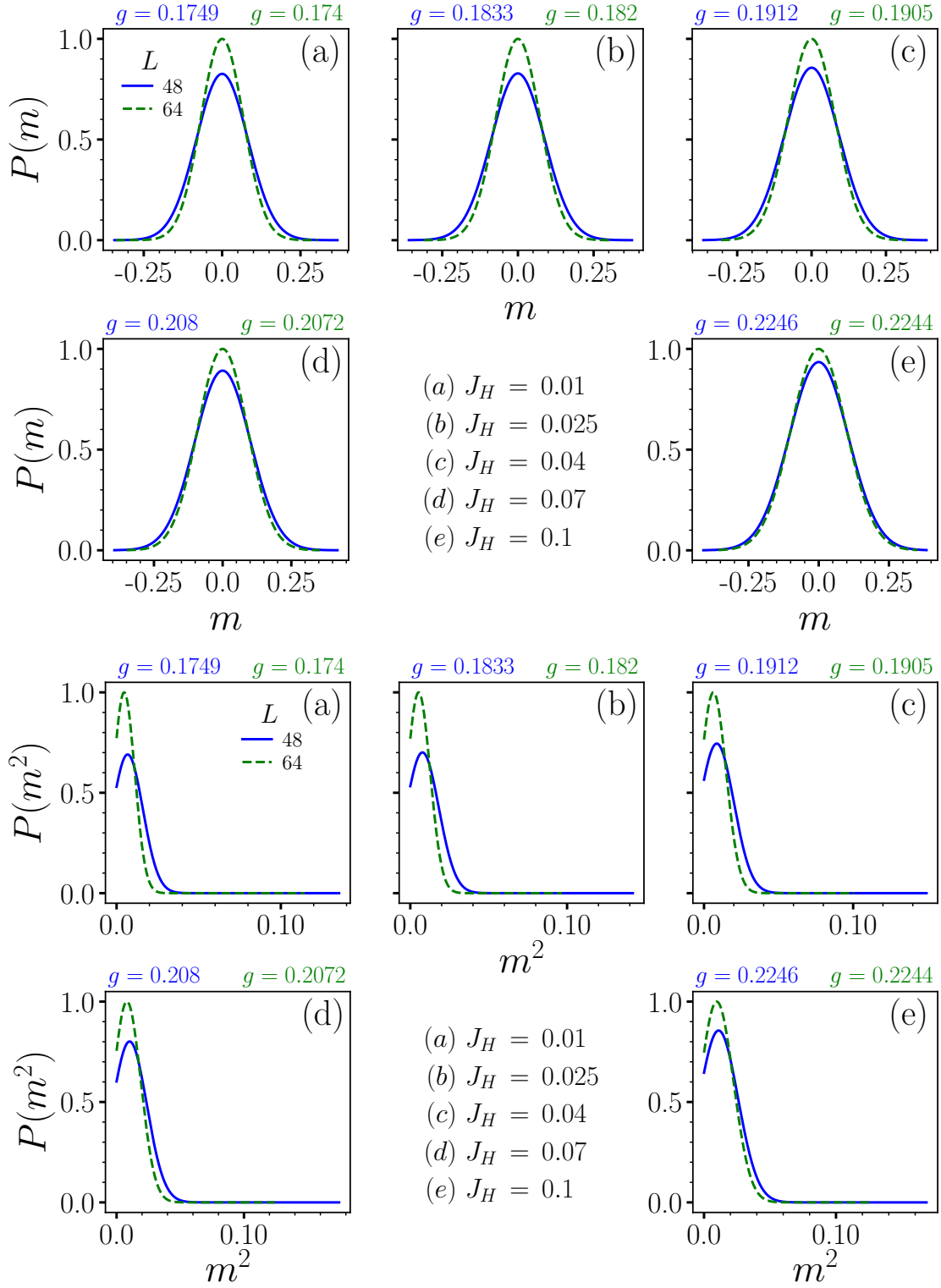


FIG. 6. This figure expands on Fig. 2a of the main text to document the various staggered magnetization histogram data collected. $\beta = \frac{L}{4}$ throughout. The g values above correspond to $\sim g_c(L)$.

D. cVBS order parameter histograms

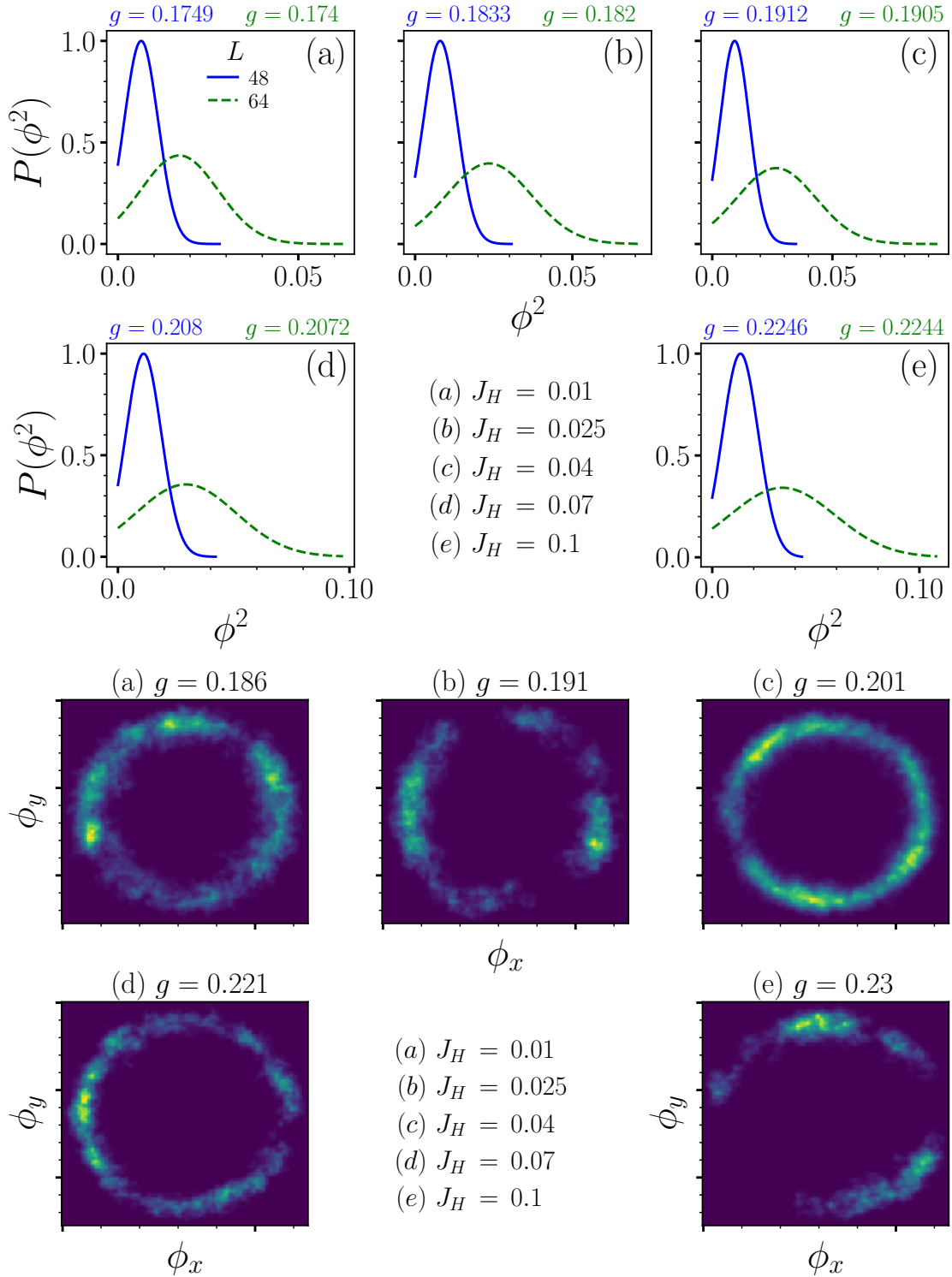


FIG. 7. This figure expands on Fig. 2b of the main text to document the various cVBS histogram data collected. $\beta = \frac{L}{4}$ throughout. $L = 64$ for cVBS (ϕ_x, ϕ_y) heat maps. The g values above correspond to $\sim g_c(L)$. For the heat maps, we have chosen g slightly to the right of $g_c(L)$ to better highlight the “ $U(1)$ -symmetric” nature of these histograms.

E. Staggered magnetization time series

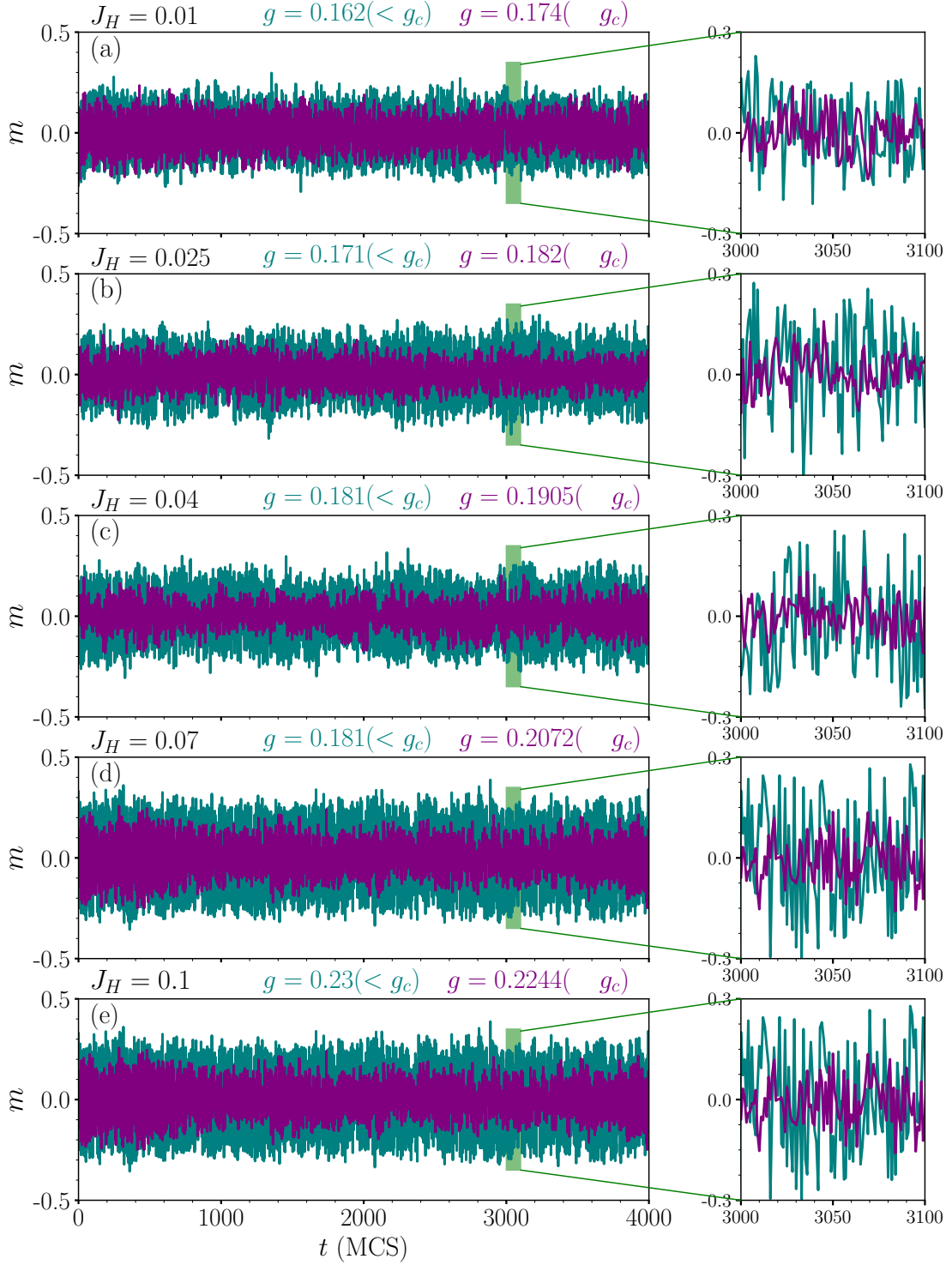


FIG. 8. This figure expands on Fig. 2c to document the various time series data collected on staggered magnetization. $\beta = \frac{L}{4}$ and $L = 64$ throughout. The time series data are in register with those in Fig. 9.

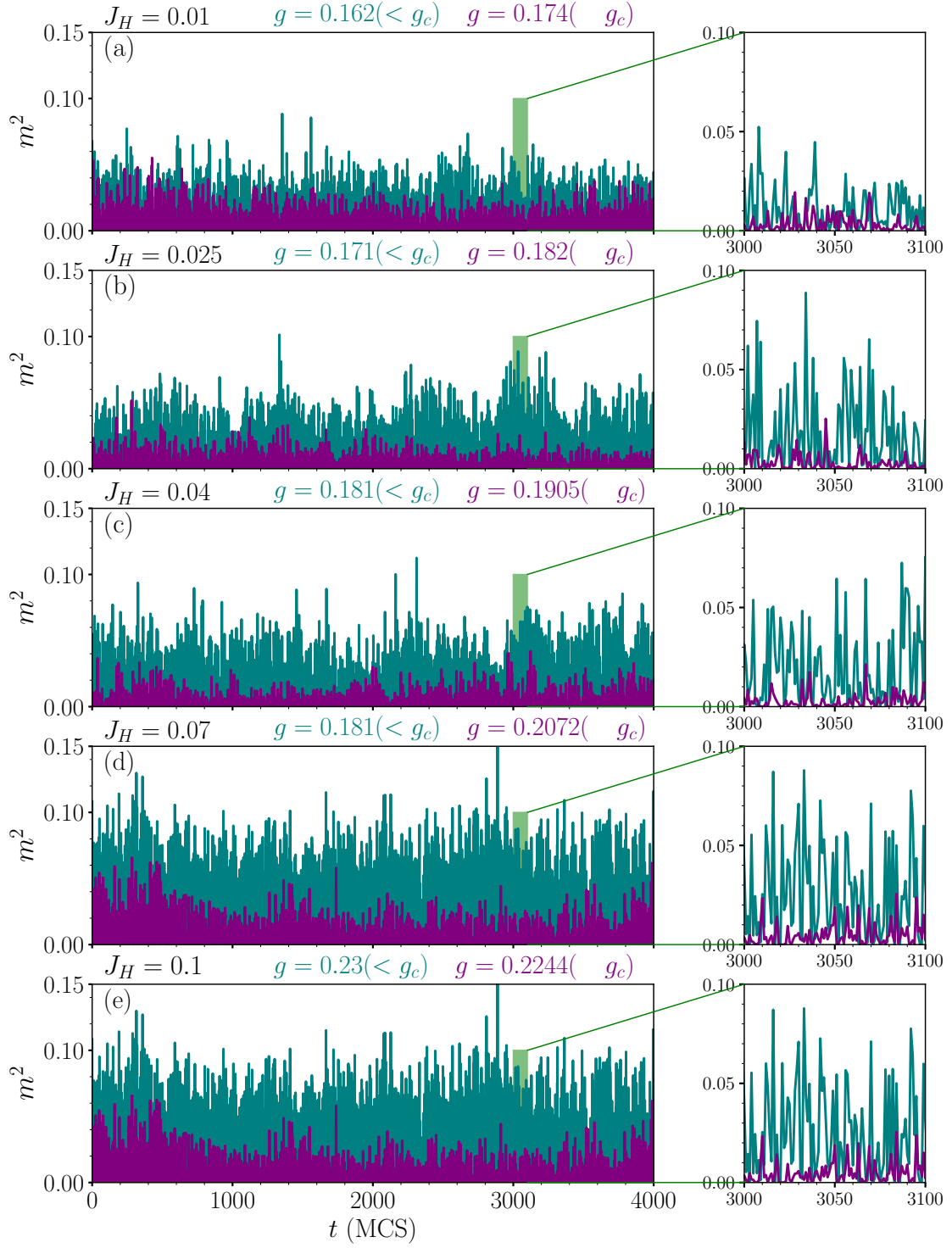


FIG. 9. This figure expands on Fig. 2c to document the various time series data collected on staggered magnetization. $\beta = \frac{L}{4}$ and $L = 64$ throughout. The time series data are in register with those in Fig. 8.

F. cVBS order parameter time series

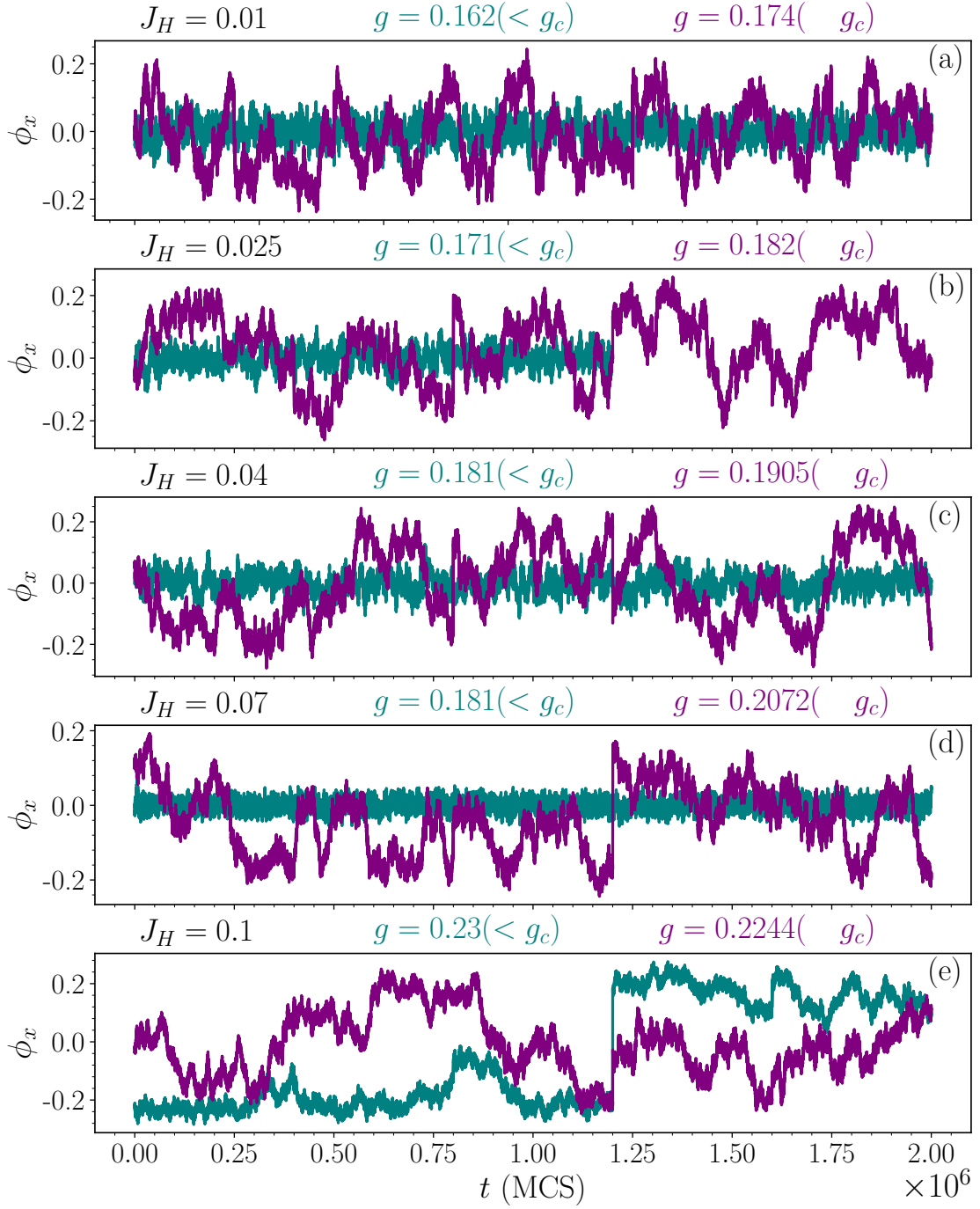


FIG. 10. This figure expands on Fig. 2 to document the various time series data collected on cVBS order parameter. $\beta = \frac{1}{4}$ and $L = 64$ throughout. The time series data are in register with those in Figs. 11,12.

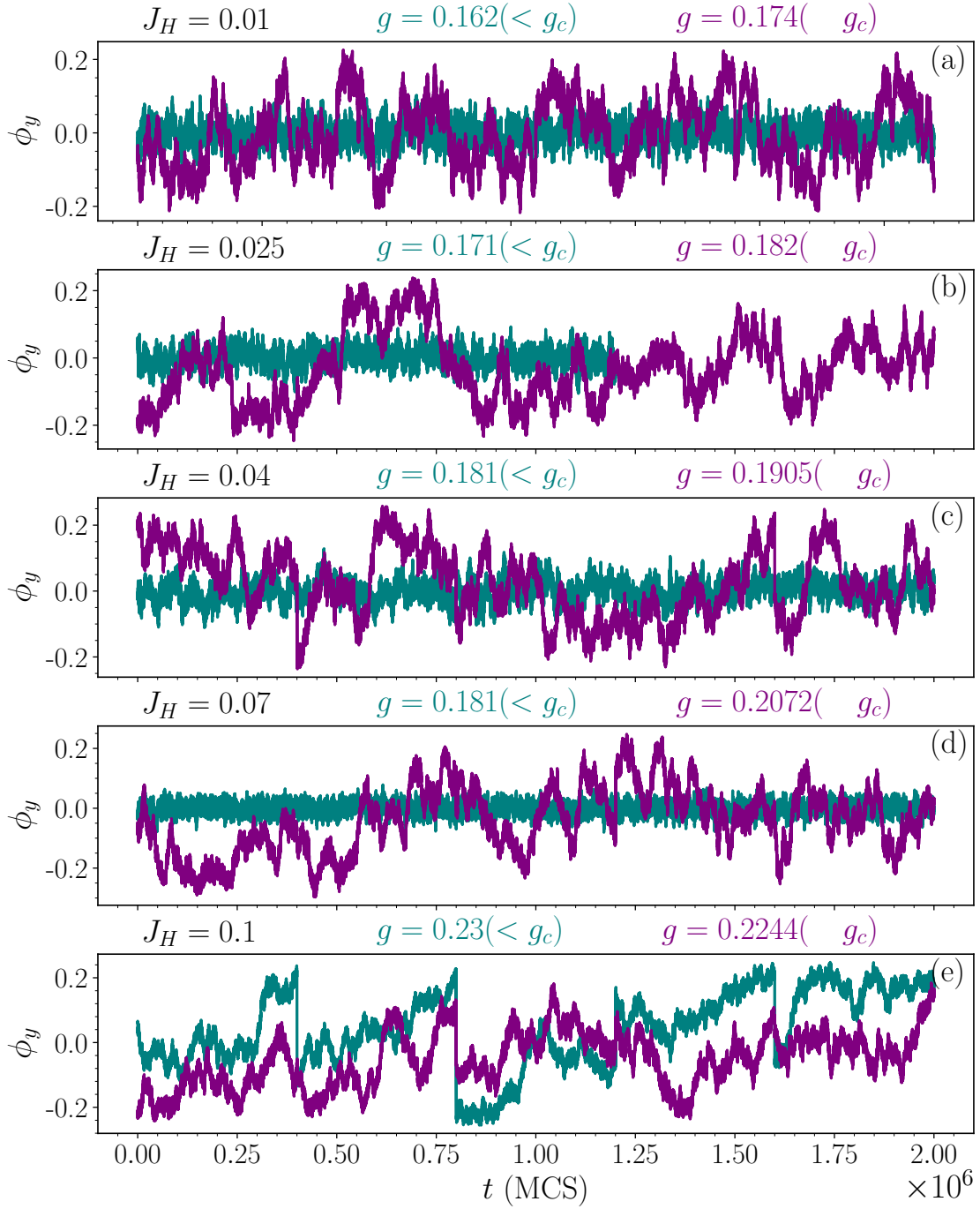


FIG. 11. This figure expands on Fig. 2 to document the various time series data collected on cVBS order parameter. $\beta = \frac{L}{4}$ and $L = 64$ throughout. The time series data are in register with those in Figs. 10,12.

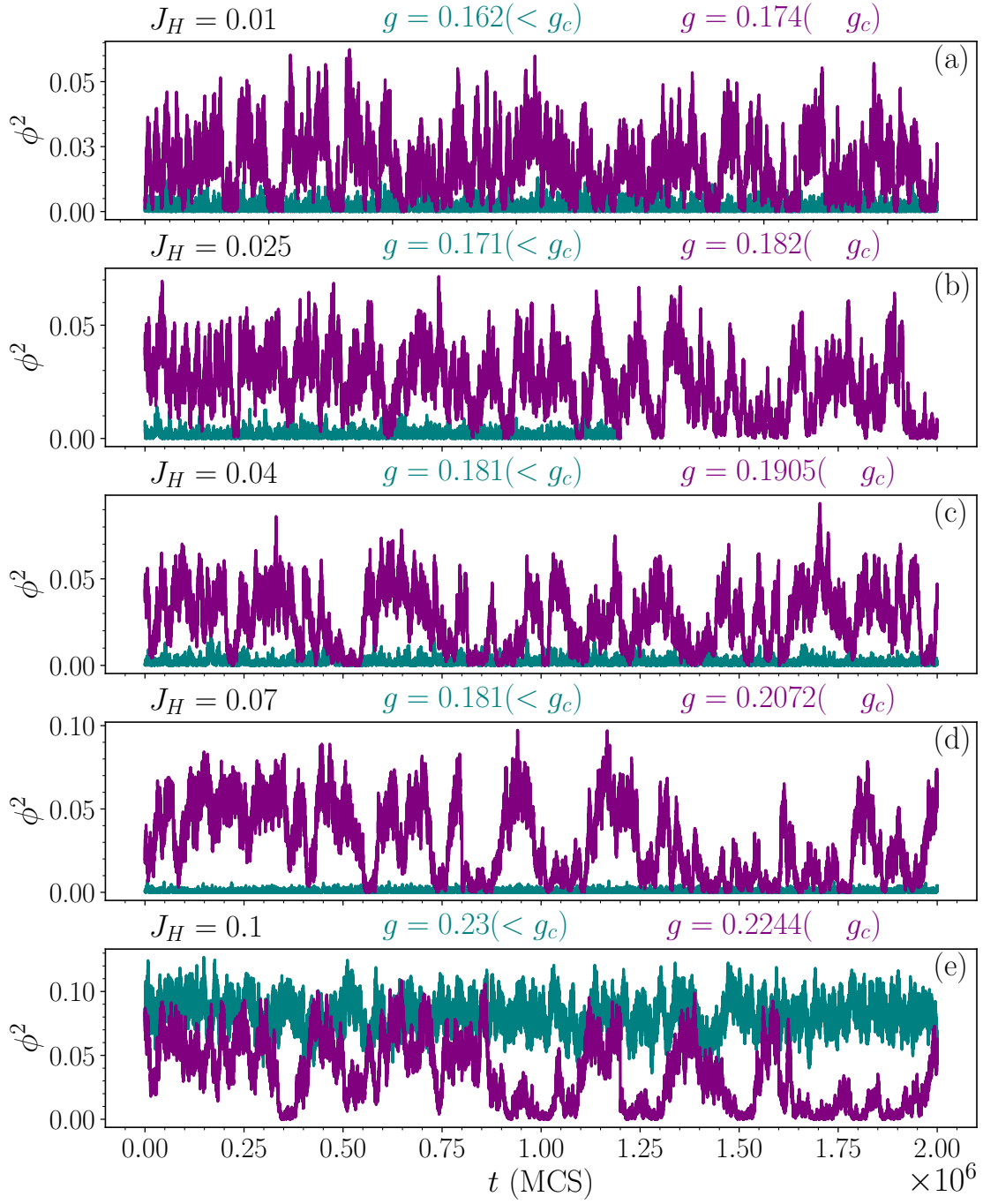


FIG. 12. This figure expands on Fig. 2 to document the various time series data collected on cVBS order parameter. $\beta = \frac{1}{4}$ and $L = 64$ throughout. The time series data are in register with those in Figs. 10,11.

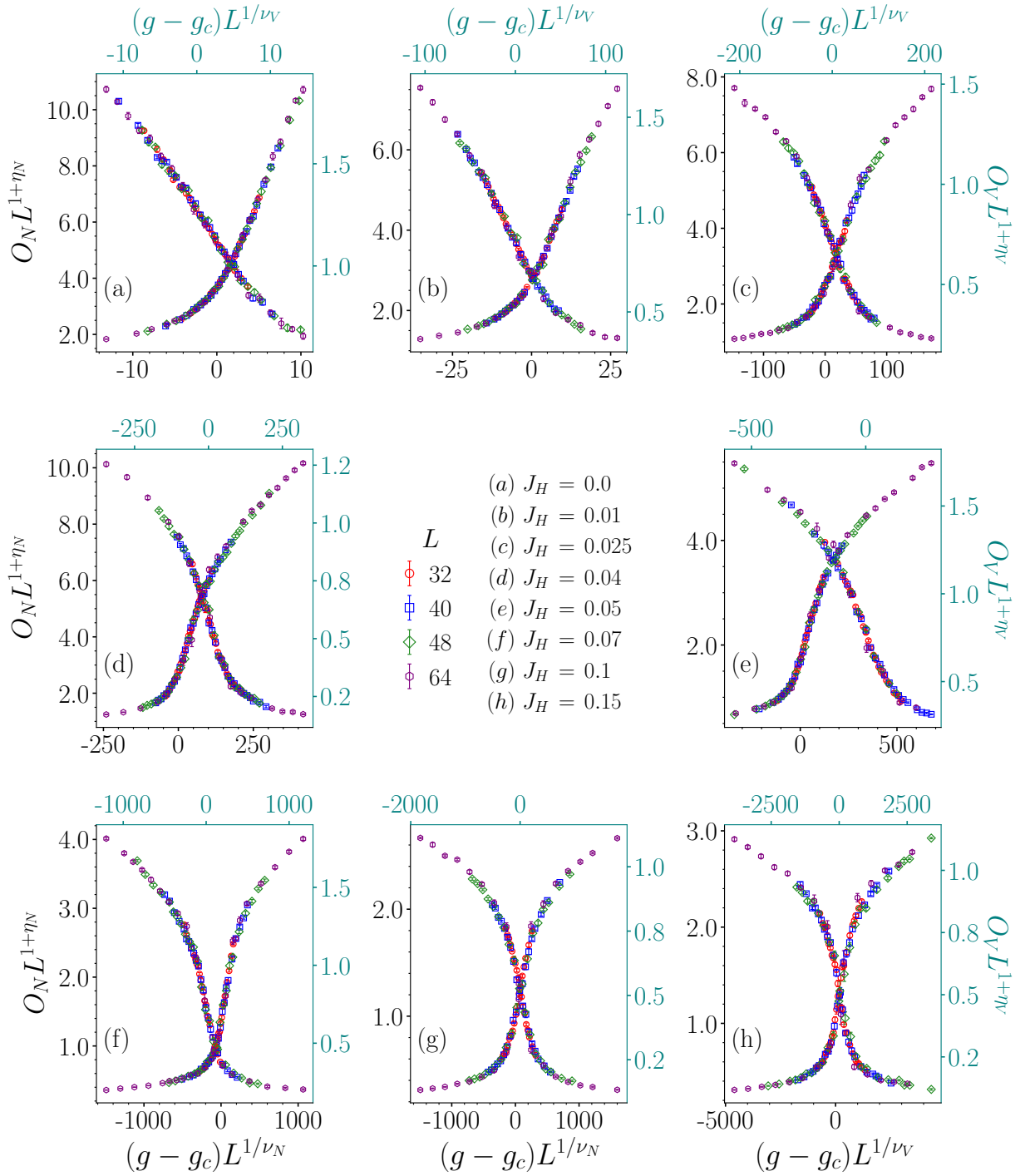


FIG. 14. This figure expands on Fig. 3c,d of the main text to document all the scaling collapse analysis performed on correlation ratios. $\beta = \frac{L}{4}$ throughout. $\beta = \frac{L}{4}$ throughout.

H. Binder Ratios

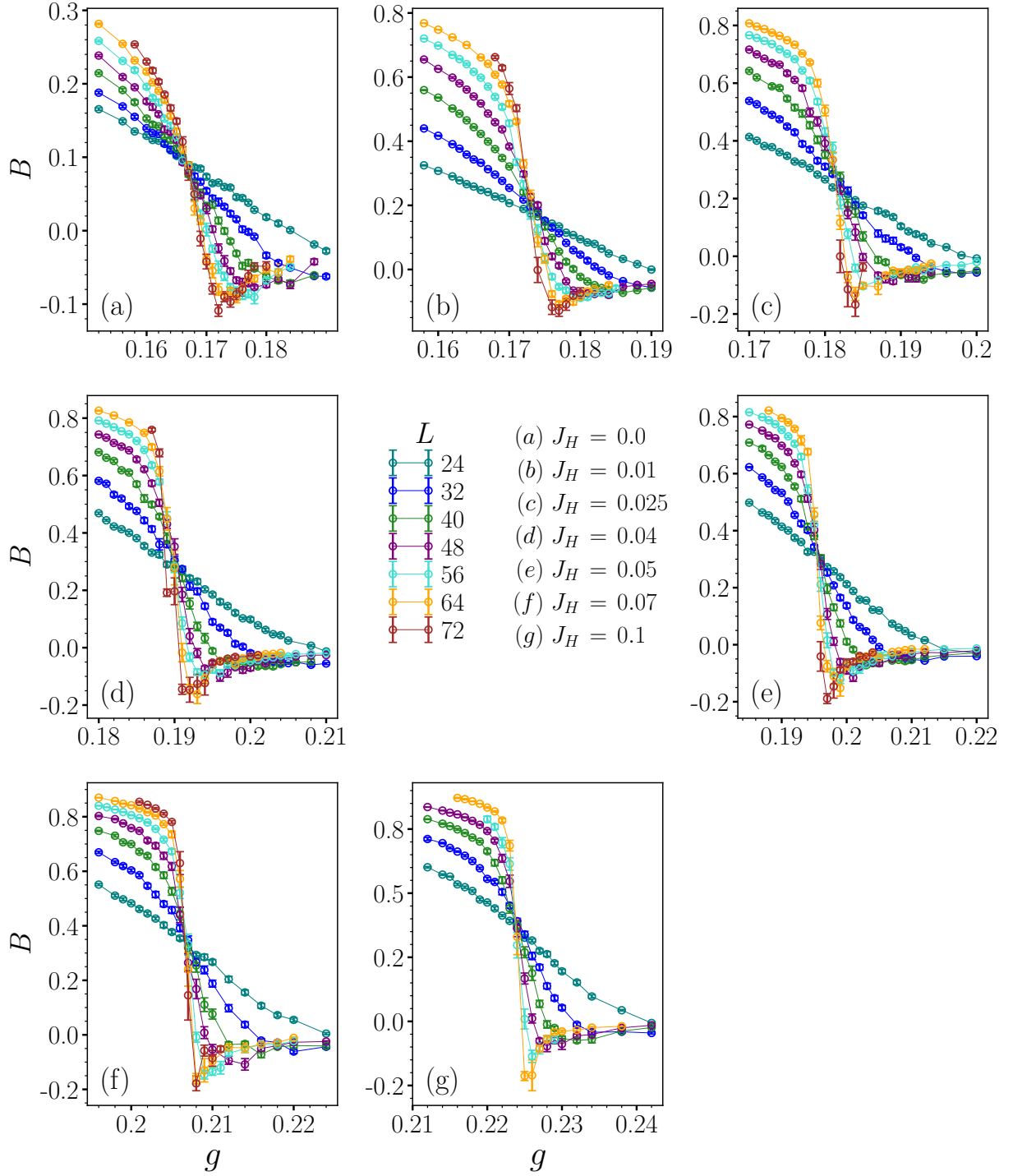


FIG. 15. This figure expands on Fig. 4 of the main text to document all the Binder ratio data collected. $\beta = \frac{L}{4}$ throughout.

III. TABLES

A. Critical exponents and critical point estimates

TABLE I. Critical exponents (ν_N, ν_V) and critical point estimates (g_{cN}, g_{cV}) as obtained after performing a scaling collapse on the Néel and cVBS correlation ratios (R_N and R_B). System sizes used for collapses are in the range of $L = 24, 32, 40, 48, 64$. $\beta = \frac{L}{4}$ throughout. Neither (ν_N, ν_V) nor (g_{cN}, g_{cV}) were set equal.

| J_H | ν_N | ν_V | g_{cN} | g_{cV} | χ_N^2 | χ_V^2 |
|-------|---------|---------|----------|----------|------------|------------|
| 0.0 | 0.49(5) | 0.63(1) | 0.168(1) | 0.167(1) | 0.9-1.56 | 1.14-1.81 |
| 0.01 | 0.41(2) | 0.56(4) | 0.175(1) | 0.171(1) | 1.31-2.27 | 1.32-1.84 |
| 0.025 | 0.40(3) | 0.51(3) | 0.182(1) | 0.18(1) | 0.97-2.43 | 1.15-1.61 |
| 0.04 | 0.37(4) | 0.49(1) | 0.191(1) | 0.188(1) | 1.12-2.64 | 1.14-1.86 |
| 0.05 | 0.40(3) | 0.46(3) | 0.196(1) | 0.195(1) | 0.91-1.78 | 1.15-1.84 |
| 0.07 | 0.34(5) | 0.48(5) | 0.207(1) | 0.206(1) | 1.52-2.54 | 1.04-1.77 |
| 0.1 | 0.31(1) | 0.40(1) | 0.225(1) | 0.223(1) | 1.55-2.27 | 1.03-2.26 |
| 0.15 | 0.32(4) | 0.44(2) | 0.254(1) | 0.252(1) | 1.37-3.39 | 0.74-1.91 |

TABLE II. Critical exponents ($\eta_V, \eta_N, \nu_N, \nu_V$) and critical point estimates (g_{cN}, g_{cV}) as obtained after performing a scaling collapse of the Néel and cVBS order parameters (O_N, O_B). System sizes used for collapses are in the range of $L = 24, 32, 40, 48, 64$. $\beta = \frac{L}{4}$ throughout. (ν_N, ν_V) were not set equal to each other, while g_{cN} and g_{cV} values were fixed while performing the scaling collapse to the values obtained from the scaling collapse of correlation ratios as shown the preceding table.

| J_H | ν_N | ν_V | η_N | η_V | g_{cN} | g_{cV} | χ_N^2 | χ_V^2 |
|-------|---------|---------|----------|----------|----------|----------|------------|------------|
| 0.0 | 0.53(3) | 0.63(1) | 0.41(1) | 0.50(2) | 0.168 | 0.167 | 1.01-1.71 | 1.67-2.53 |
| 0.01 | 0.45(3) | 0.54(3) | 0.26(2) | 0.46(2) | 0.174 | 0.171 | 1.45-1.66 | 1.74-2.29 |
| 0.025 | 0.43(3) | 0.46(4) | 0.21(3) | 0.33(1) | 0.182 | 0.180 | 1.04-1.55 | 0.86-1.37 |
| 0.04 | 0.40(2) | 0.43(5) | 0.24(2) | 0.23(2) | 0.191 | 0.189 | 1.99-2.28 | 1.49-2.77 |
| 0.05 | 0.39(4) | 0.38(5) | 0.16(3) | 0.17(3) | 0.196 | 0.195 | 1.28-1.54 | 0.98-1.9 |
| 0.07 | 0.38(2) | 0.36(2) | 0.05(1) | 0.12(3) | 0.207 | 0.206 | 1.67-2.35 | 2.2-2.68 |
| 0.1 | 0.33(2) | 0.41(2) | 0.12(2) | 0.28(7) | 0.225 | 0.223 | 2.48-2.81 | 2.55-2.86 |
| 0.15 | ?? | ?? | ?? | ?? | 0.254 | 0.252 | ?? | ?? |

TABLE III. Critical exponents ($\eta_V, \eta_N, \nu_N, \nu_V$) and critical point estimates (g_{cN}, g_{cV}) as obtained after performing a scaling collapse of Néel and cVBS order parameters (O_N, O_B) for eight sets of the Heisenberg strength, $J_H = 0, 0.01, 0.025, 0.04, 0.05, 0.07, 0.1, 0.15$. System sizes used for collapses are in the range of $L = 24, 32, 40, 48, 64$. $\beta = \frac{L}{4}$ throughout. Neither (ν_N, ν_V) nor (g_{cN}, g_{cV}) were set equal. This table was presented in the main text as well, and the estimates of various fitting parameters below are corroborated well by the estimates from the preceding tables.

| J_H | ν_N | ν_V | η_N | η_V | g_{cN} | g_{cV} | χ_N^2 | χ_V^2 |
|-------|---------|---------|----------|----------|----------|----------|------------|------------|
| 0.0 | 0.53(3) | 0.63(1) | 0.44(5) | 0.49(2) | 0.168(1) | 0.167(1) | 1.08-1.68 | 1.69-2.46 |
| 0.01 | 0.45(2) | 0.54(3) | 0.23(3) | 0.42(4) | 0.174(1) | 0.171(1) | 1.19-1.63 | 1.38-1.73 |
| 0.025 | 0.43(3) | 0.46(4) | 0.15(9) | 0.38(2) | 0.182(1) | 0.180(1) | 0.75-1.46 | 0.8-1.4 |
| 0.04 | 0.40(2) | 0.43(5) | 0.13(7) | 0.30(8) | 0.19(1) | 0.189(1) | 1.06-1.67 | 1.09-1.5 |
| 0.05 | 0.39(4) | 0.38(5) | 0.20(9) | 0.29(6) | 0.196(1) | 0.195(1) | 0.87-1.31 | 0.87-1.96 |
| 0.07 | 0.38(2) | 0.39(3) | 0.10(4) | 0.10(4) | 0.207(1) | 0.206(1) | 1.52-2.54 | 1.04-1.77 |
| 0.1 | 0.35(4) | 0.35(3) | -0.03(5) | -0.03(2) | 0.224(1) | 0.224(1) | 1.24-3.28 | 0.99-1.97 |
| 0.15 | 0.33(2) | 0.33(1) | 0.00(8) | -0.12(8) | 0.253(1) | 0.253(1) | 1.42-1.79 | 1.15-1.63 |

B. Benchmarking with Exact Diagonalization

TABLE IV. This benchmarking table shows the values of total energy (E), Néel observables (O_N , R_N) obtained by Exact diagonalization (ED) and SSE-QMC on a 2×2 square plaquette at $\beta = 10$.

| (J_B, Q_B, J_H) | E^{ED} | E^{SSE} | O_N^{ED} | O_N^{SSE} | R_N^{ED} | R_N^{SSE} |
|-------------------|-----------------|------------------|-------------------|--------------------|-------------------|--------------------|
| (1.0,1.0,0.2) | -5.4524 | -5.452(5) | 1.6980 | 1.6980(2) | 0.35739 | 0.3573(9) |
| (0.9,0.4,0.3) | -3.6835 | -3.683(2) | 1.7386 | 1.738(5) | 0.36655 | 0.3665(4) |
| (0.6,0.5,0.5) | -3.8492 | -3.849(0) | 1.7849 | 1.785(2) | 0.37651 | 0.3765(3) |
| (0.3,0.8,0.2) | -3.4539 | -3.4539(6) | 1.7170 | 1.717(1) | 0.36172 | 0.3617(1) |
| (1.15,0.88,0.12) | -5.2108 | -5.210(7) | 1.6861 | 1.686(2) | 0.35463 | 0.3546(0) |

TABLE V. This benchmarking table shows the values of VBS observables (O_V , R_V , O_B , R_B) obtained by Exact diagonalization (ED) and SSE-QMC on a 2×2 square plaquette at $\beta = 10$.

| (J_B, Q_B, J_H) | O_V^{ED} | O_V^{SSE} | R_V^{ED} | R_V^{SSE} | O_B^{ED} | O_B^{SSE} | R_B^{ED} | R_B^{SSE} |
|-------------------|-------------------|--------------------|-------------------|--------------------|-------------------|--------------------|-------------------|--------------------|
| (1.0,1.0,0.2) | 1.63654 | 1.6365(4) | 0.5 | 0.4999(5) | 1.49930 | 1.4993(3) | 0.5 | 0.5000(1) |
| (0.9,0.4,0.3) | 1.65070 | 1.6507(4) | 0.5 | 0.4999(8) | 1.49615 | 1.496(2) | 0.5 | 0.49999(8) |
| (0.6,0.5,0.5) | 1.66564 | 1.665(5) | 0.5 | 0.49999(7) | 1.48881 | 1.488(8) | 0.5 | 0.4999(9) |
| (0.3,0.8,0.2) | 1.64326 | 1.643(4) | 0.5 | 0.4999(9) | 1.49817 | 1.498(0) | 0.5 | 0.5000(3) |
| (1.15,0.88,0.12) | 1.63223 | 1.632(1) | 0.5 | 0.4999(5) | 1.49973 | 1.499(8) | 0.5 | 0.49999(3) |